

A Molecular Dynamics Study on CO₂ Diffusion Coefficient in Saline Water Under a Wide Range of Temperatures, Pressures, and Salinity Concentrations: Implications to CO₂ Geological Storage

Sina Omrani^{a†}, Mehdi Ghasemi^{b†}, Saeed Mahmoodpour^{c*}, Ali Shafiei^{b*}, Behzad Rostami^a

^a *Institute of Petroleum Engineering, College of Engineering, University of Tehran, Tehran, Iran.*

^b *Petroleum Engineering Program, School of Mining & Geosciences, Nazarbayev University, Nur-Sultan, Astana 010000, Kazakhstan*

^c *Institute of Applied Geosciences, Geothermal Science and Technology, Technische Universität Darmstadt, Darmstadt, Germany*

[†] *S. Omrani and M.Ghasemi contributed equally to this work.*

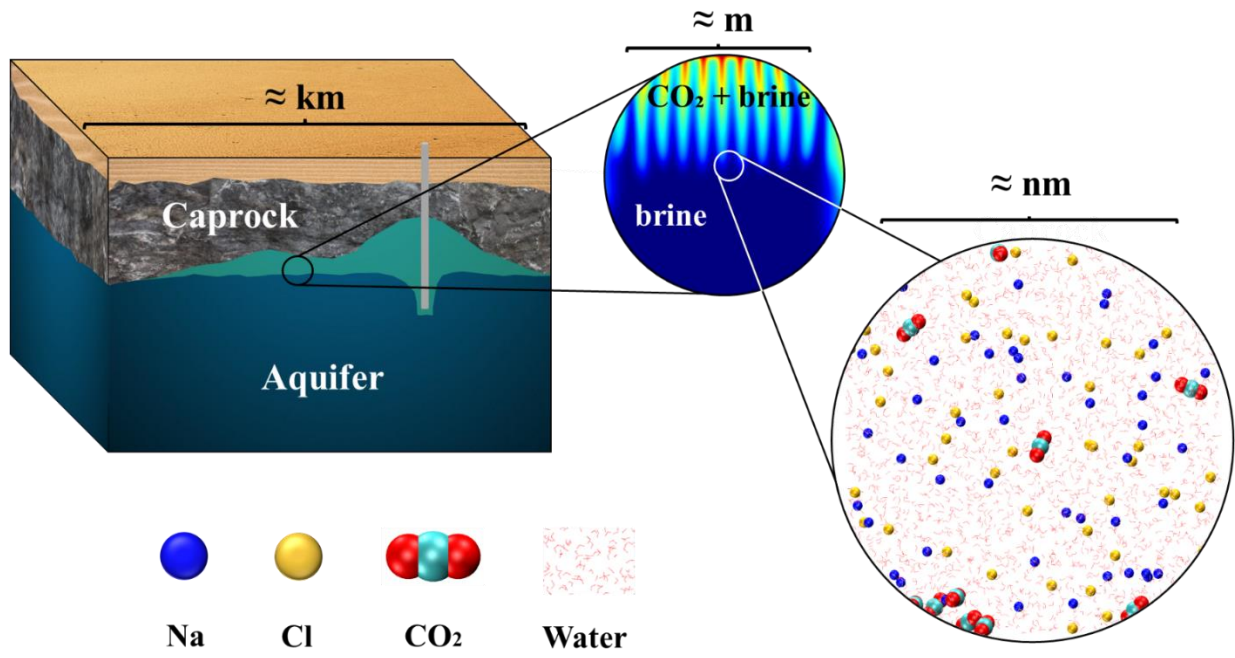
** Corresponding authors*

E-mail addresses: saeed.mahmoodpour@tu-darmstadt.de (S. Mahmoodpour), ali.shafiei@nu.kz.edu (A. Shafiei)

Highlights

- The CO₂ diffusion coefficient monotonically decreases with increasing NaCl concentration.
- At higher temperatures, the CO₂ diffusion coefficient degree of reduction is more severe.
- Pressure has a relatively negligible impact on the CO₂ diffusion coefficient in water/brine.

Graphical Abstract



Abstract

Carbon dioxide (CO₂) sequestration in saline aquifers has been introduced as one of the most practical, long-term, and safe solutions to tackle a growing threat originating from the emission of CO₂. Successfully executing and planning the process necessitates a comprehensive understanding of CO₂ transport properties—particularly the diffusion coefficient, influencing the behavior of CO₂ dissolution in water/brine regarding the shape of viscous fingers, the onset of instabilities, etc. In this research, Molecular Dynamics (MD) simulation was employed to compute the CO₂ diffusion coefficient in various NaCl saline water concentrations (1-6 mol NaCl/kg water) under the broad spectrum of temperatures (294-423 K) and pressures (10-30 MPa) to acquire a data-set for the CO₂ diffusion coefficient in different circumstances. According to the results, the NaCl concentration increase gives rise to a decrease in the CO₂ diffusion coefficient, by which the reduction is most notably at higher temperatures. In fact, the presence of more cations due to the salinity concentration increase forms further hydration shells, acting as a barrier for CO₂ diffusion. In addition, the rise in the CO₂ diffusion at elevated temperatures can be explained by the cation's hydration shell size reduction with temperature increment due to intensifying repulsive forces among water molecules. We also proposed a new precise correlation for estimating CO₂ diffusion coefficients over temperatures and salinity ranges of this study. Regarding the pressure variation effects, no tangible changes are observed with pressure increase, validating a negligible influence on the diffusion coefficient. Furthermore, the variability of the CO₂ diffusion coefficient in the presence of other salts, namely MgCl₂, CaCl₂, KCl, and Na₂SO₄, were computed separately. Comparing the influence of various salts, CaCl₂ and KCl have the highest and lowest effect on the CO₂ diffusion coefficient, respectively. Finally, a set of direct numerical simulations was conducted to study the impact of the CO₂ diffusion coefficient on the CO₂ dissolution process. The results shed light on the importance of CO₂ diffusion coefficient changes under the saline water condition in predicting dissolution process behavior and further calculations.

Keywords: Diffusion Coefficient, CO₂ Storage, Saline Aquifers, Molecular Dynamics Simulation.

1. Introduction

The increase of greenhouse gases, in particular carbon dioxide (CO₂), has become a severe challenge that puts the life of most species in danger. To minimize CO₂ emission in the environment, a promising solution of CO₂ storage in saline aquifers has been introduced as a viable option due to the high capacity, chemistry, and geological accessibility of saline aquifers [1-3]. In order to have long-term safety of underground CO₂ storage, a thorough assessment of trapping mechanisms in the saline aquifers is essential [4]. In this regard, the CO₂ dissolution mechanism is considered a necessity among trapping mechanisms to bring about enduring CO₂ storage [5]. The dissolution process initiates with CO₂ diffusion into brine. The relatively higher density of the newly formed diffuse layer of CO₂ and brine on top of an aquifer compared to the original brine (i.e., brine without the dissolved CO₂) results in gravitational instabilities. These instabilities grow with time and eventuate to the convective fingers, which gradually move downward. The replacement with fresh brine is continued until the aquifer reaches its maximum dissolution capacity and can no longer dissolve more CO₂. Dissolution of CO₂ from one aspect prepares the conditions for the permanent storage of the CO₂ through mineralization. From the other aspect, it decreases the stress on the caprock through pressure reduction. Furthermore, dissolved CO₂ has a higher viscosity and density compared to the gas phase, and the possibility of leakage would decrease. Therefore, the higher CO₂ dissolution rate into the brine reduces leakage risk.

The behavior of the dissolution process in terms of instability onset, the shape and number of convective fingers, and dissolution flux is considerably affected by the diffusion coefficient and its controlling parameters such as temperature, pressure, salinity, etc., during the whole diffusion-convection process. The role of salinity or impurities in CO₂ diffusion coefficient changes has been ignored in previous works, in which either the CO₂ diffusion coefficient in pure water was used [6-9], the works have been limited to a range of available data [10], or they tried to calculate effective diffusion coefficient based on experimental results [11]. Nevertheless, limited studies have attempted to assess the CO₂ diffusion coefficient in water in the presence of various impurities and salts [12-18]. A summary of the literature is provided hereunder.

In earlier research regarding CO₂ storage in an aquifer, measurement of the CO₂ diffusion in pure water under a short range of temperature and pressure was the center of attention [19-25]. Nevertheless, over time, studies have used better techniques to measure CO₂ diffusion coefficients. In 1994, Tamimi et al. [26] used a wetted-sphere absorption apparatus to measure the diffusion coefficients for H₂S, CO₂, and N₂O in water at the temperature range of 293-368 K. Hirai et al. [27] predicted the CO₂ diffusion coefficient by measuring the liquid CO₂ droplet-dissolution rate. In 2012, Sell et al. [15] used a microfluidic-based approach to measure the CO₂ diffusion coefficient in water and NaCl brine. They measured CO₂ diffusion in brine at 299 K, 0.5 MPa, and up to 5 molars (M) NaCl concentration and proposed an exponential relationship between the diffusion coefficient and salinity. In 2014, Cadogan et al. [28] measured CO₂ and N₂ diffusion coefficients for a broad spectrum of temperatures and pressure via the Taylor dispersion method. In 2015, their research team measured the CO₂ diffusion coefficient in brine at 298 K and 0.1 bar MPa using Nuclear Magnetic Resonance (NMR) method. Several types of salts were also investigated (NaCl, CaCl₂, and Na₂SO₄) [29]. Zhang et al. [16] used the pressure decay method to measure the CO₂ diffusion coefficient. They evaluated the effect of temperature, pressure, salt concentration, and type of salt on the CO₂ diffusion coefficient. Their study showed that the diffusion coefficient increases by increasing temperature or pressure while decreasing with salinity. Belgodere et al. [17] applied Raman spectroscopy to compute the CO₂ diffusion coefficient in pressurized aqueous solution (both pure and saline water) at room temperature. They also claimed the inverse relationship of the CO₂ diffusion coefficient with salinity. Jafari Raad et al. [4] also measured the CO₂ diffusion coefficient in pure and saline water under an extensive range of temperature and pressures by employing the pressure decay method. The Supporting Information (SI) provides a list of previous works done on this subject in **Table S1**.

The experimental measurement of the diffusion coefficient entails a complex and time-consuming procedure. Therefore, finding a great alternative technique is vital. With the advent of computational methodologies, Molecular Dynamics (MD) simulation has been demonstrated as a valuable method for evaluating physicochemical characteristics and fluids' thermodynamic and transport properties [30-32]. Heretofore, it has been established that MD simulations can be used to calculate diffusion coefficients [33,

34]. For example, Garcia-Rates et al. [35] employed MD simulation to estimate the CO₂ diffusion coefficient in NaCl brine under the influence of temperature (333.15, 393.15, and 453.15 K), pressure (10 and 20 MPa), and salinity (1, 2, and 4 M). They observed that an increase in the temperature causes the diffusion coefficient increment, while no accurate relationship is present for the dependency of the diffusion coefficient on salinity or CO₂ concentration. Moulton et al. [36] estimated the CO₂ diffusion coefficient via MD simulations, as well. They compared diverse combinations of force fields for CO₂ (EPM2 and TraPPE) and water (SPC, SPC/E, and TIP4P/2005) by considering various temperatures and pressures. Finally, they proposed a correlation for predicting the CO₂ diffusion coefficient in water.

To the best of the authors' knowledge, although some researchers have emphasized the impact of salinity on the diffusion coefficient variation, the literature lacks a comprehensive set of CO₂ diffusion coefficient data in saline water in a comprehensive range of temperatures, pressures, and salt concentrations. In this research, we aimed to apply MD simulations to estimate the CO₂ diffusion coefficient at the temperature and pressure range of 294-423 K and 10-30 MPa, respectively, under NaCl concentrations of 1, 2, 4, and 6 M. Further investigation was conducted to scrutinize the effect of 4 different types of salt, including MgCl₂, CaCl₂, KCl, and Na₂SO₄, on the diffusion coefficient, and then compared with the NaCl. Next, according to the obtained values, we proposed a novel correlation to predict the CO₂ diffusion coefficient in saline brine, which can be valuable in engineering applications. In the final stage, to clarify the influence of ignoring the dependency of the CO₂ diffusion coefficient on salinity and assuming the CO₂ diffusion coefficient value in pure water instead, we analyzed the CO₂ dissolution behavior using direct numerical simulation at a temperature of 323 K. The primary aim of the study is to provide some reliable data, which can serve as a reference, to enhance the accuracy of Carbon Capture and Sequestration/Storage (CCS) planning and executing.

The remainder of this paper is organized as follows. First, we described the theory of diffusion coefficient calculation and details of the MD simulations in Section 2. Then, results and in-depth interpretation of analyses were provided in Section 3. Finally, the conclusions of the research were drawn in section 4.

2. Methodology

In this section, we first described the different diffusion coefficient types and their calculation methods via MD simulation results, and then we discussed details of the simulation procedure.

2.1. Diffusion and Related Theories

Mass transfer computation requires an accurate description of the diffusion coefficient and thus diffusion mechanism. Diffusion coefficients are classified as follows: 1) Self-diffusion coefficient (D_{Self}), which describes the transport of particles due to Brownian motion, 2) Maxwell-Stefan (MS) diffusion coefficient (D_{MS}) that represents friction between two components, and 3) Fick diffusion coefficient (D_{Fick}), which is resulting from the concentration gradient of a component [12]. The diffusion coefficient of different kinds can be studied and validated with two different MD simulation methods: equilibrium MD (EMD) and non-equilibrium MD (NEMD). There is a difference between these two methods in whether the external force is present or not. Generally, due to some problems existing in the NEMD method, the EMD method, which is based on analyzing the equilibrium fluctuations, has been more widely adopted to calculate the diffusion coefficient [31, 37, 38]. Calculating the D_{Self} , as a concern of this study, using MD can be predicted following two methods: Einstein and Green-Kubo [39]. According to the literature, the Einstein method is more widely preferred [12], and it is defined as follows:

$$D_{i,\text{self}} = \frac{1}{6N_i} \lim_{m \rightarrow \infty} \frac{1}{m \cdot \Delta t} \left\langle \sum_{l=1}^{N_i} \left(r_{l,i}(t + m \cdot \Delta t) - r_{l,i}(t) \right)^2 \right\rangle \quad (1)$$

where N_i is the number of particles in component i , m is the number of time steps, Δt is time step used in simulation, and $r_{l,i}(t)$ is the position of molecules l^{th} of component at time t .

Since the concept of collective diffusivities (D_{MS} and D_{Fick}) is more interesting in engineering applications, a component's net transport in a multicomponent mixture can be explained by means of collective diffusion [34]. In spite of D_{Fick} , D_{MS} cannot be measured experimentally, and the thermodynamic correction factor (Γ) relates these two theories (see Eq. (2) or a binary system). In an infinitely diluted system (which Γ is almost unity), all of these values are approximately equal [28, 40].

$$[D_{Fick}] = [D_{MS}][\Gamma] \quad (2)$$

According to the study conducted by Garcia-Rates et al. [35], a CO₂ brine system is thermodynamically ideal. As well, we calculated the Γ for some of our systems and have found similar results. We refer you to our previous paper for more details on the diffusion coefficient types and how to calculate them using MD [12].

2.2. Simulation Details

2.2.1. Molecular Dynamics (MD) Simulation

MD simulation technique, as a powerful gadget, can be employed to have a better understanding of the behavior and characteristics of simple and/or complex systems from the atomic level, particularly calculating the CO₂ diffusion coefficient in this study. Since the accuracy of MD simulation results is strongly dependent on the applied intra-intermolecular potentials, first, we conducted comparative MD simulations to determine the most precise force field for the CO₂ at infinite dilution in the saline brine system. Thus, three different developed force fields for CO₂, namely rigid and flexible TraPPE models and the EPM2 model [41-43], and two salt models of Smith and Dang and Joung and Cheatham (we refer to them as Smith and JC models, respectively) [44, 45] in combination with the SPCE model [46] for water molecules were employed to identify the combined potentials with the highest accuracy. The basis of comparison was the available CO₂ diffusion coefficient data in the literature obtained by Belgodere et al. [17] via the experimental measurement. According to the several statistical analyses [47], including average percent relative error (APRE), average percent absolute relative error (AAPRE), standard deviation (SD) of error, and root mean square error (RSME) and coefficient of determination (R^2), the combined TraPPE (Flex)-JC-SPCE potentials showed the best fit with the literature data for almost all cases, and it was selected for the rest of the simulations. Note that the SI provides the results of statistical analyses in more detail.

All MD simulations were performed by the GROMACS package (version 2021.1) [48]. A cubic box with the size of 4.5×4.5×4.5 nm³ was selected, and the periodic boundary condition (PBC) was applied in all directions. Each system followed three simulation steps: initially, the energy minimization using steepest

descent algorithm to reduce bad contacts and produce stable configuration for simulation, then the constant isothermal-isobaric ensemble (NPT) run for 3 ns to reach the desired temperature and pressure, and finally, the canonical ensemble (NVT) simulation for 60 ns to collect the data. A Nosé–Hoover thermostats and a Parrinello–Rahman barostat were applied to maintain the temperature and pressure, respectively [49-51]. The long-range electrostatic interactions were calculated using the particle-mesh Ewald (PME) summation technique with a precision of 10^{-4} . A cut-off radius of 1.2 nm was assigned for both van der Waals (vdW) and electrostatic interactions. Also, all hydrogen bonds were constrained by the Linear Constraint Solver (LINCS) algorithm [52]. Regarding the intermolecular interactions, for all cases except EPM2, which originally used geometric mean, the interactions between molecules were computed using Lorenz-Berthelot mixing rules [53]. It is worth mentioning that all simulations were repeated three times to enhance the accuracy of the results.

Note that since the finite-size simulation box impacts the diffusion coefficient calculated by MD simulations [34, 54], two other sizes of 3 and 7 nm were considered to track the changes in diffusion coefficient values (see **Figure S1**). According to the results, although the variation in the diffusion coefficients was relatively negligible, we corrected even the small effect (almost 2 orders of magnitude lower than the diffusion coefficient) by the Yeh–Hummer method [55].

$$D_{\text{Self}} = D_{\text{Self}}^{\text{MD}} + \frac{k_{\text{B}}T\xi}{6\pi\eta L} \quad (3)$$

where k_{B} and T are the Boltzmann constant and temperature, respectively. ξ is a dimensionless constant equal to 2.837298 for periodic cubic boxes, η is the shear viscosity, and L is the box size in nm.

2.2.2. Direct Numerical Simulation

To clarify the dependency of CO_2 dissolution behavior on the diffusion coefficient in saline brine, we applied direct numerical simulation based on the finite element method using COMSOL software. We chose cases at 323 K and 10 MPa. To capture the dissolution behavior, the following equations as the mass transfer (Eq. (4)) and continuity (Eq. 5a) equations should be solved in a fully coupled scheme:

$$\phi \frac{\partial C}{\partial t} = \phi \nabla \cdot (D \nabla C) - V \cdot \nabla C \quad (4)$$

$$\nabla U = 0 \quad (5a)$$

$$U = -\frac{k}{\mu} (\nabla P - \rho g) \quad (5b)$$

where ϕ , C , D , U , k , P , μ , ρ , and g represent porosity, dissolved CO₂ concentration, diffusion coefficient, the Darcy velocity vector, permeability, pressure, the viscosity, the density, and the gravity acceleration constant, respectively. Duan and Sun paper was used to get the solubility of CO₂ in water/brine [56]. We applied the Garcia method to calculate the CO₂-rich brine density [57], and the density and viscosity of brine were computed by Mao and Daun [58, 59]. We used an equation from our previous work to estimate the onset of the shut-down regime to determine how long each simulation should be continued [60]. Our previous papers entail more detail on the direct numerical simulation [11, 61]. These equations are solved once with the diffusion coefficients calculated from this study and again with considering the CO₂ diffusion coefficient in pure water in order to demonstrate their impact on CO₂ dissolution process behavior.

3. Results and Discussion

In this section, the CO₂ diffusion coefficient values in brine under various conditions are calculated. The impact of four factors, namely NaCl salinity concentration, temperature, pressure, and salinity type, were scrutinized. The radial distribution function (RDF) and H-bonds analyses were also discussed to elucidate the reason behind the results.

3.1. CO₂ Diffusion Coefficient Under Various NaCl Salinities and Temperatures

The combined effects of temperature and salinity alteration on the CO₂ diffusion coefficient are shown in **Figure 1**. In order to better visualize the trends, we categorized the results into relatively low and high temperatures (**Figure 1a** and **b**, respectively). Generally, there is a similar consensus over the impacts of temperature and salinity on the diffusion coefficient. A rise in temperature results in greater kinematic energy and, therefore, a higher diffusion coefficient, while an increase in NaCl salinity results in a lower diffusion coefficient. In more detail, the salinity increment brings about a monotonical reduction of the diffusion

coefficient, by which the reduction is more severe at the beginning of curves for higher temperatures. Compared to pure water, the CO₂ diffusion coefficient in brine is reduced, on average, by 15%, 29%, 49%, and 64%, respectively, at 1 M, 2 M, 4 M, and 6 M solutions. Since the trend follows an exponential behavior at each temperature, a regression analysis was performed using an optimization code in Python to provide a correlation between the CO₂ diffusion coefficients in an aqueous solution at temperatures ranging from 294 to 423 K and NaCl concentrations of 0 to 6 M.

$$\text{Diffusion Coefficient} = -18.157948 \times e^{-0.05736C} + 0.068700205361 \times T - 0.068700205361 \times C^{0.820561458} \times T^{1.46331515077} \quad (6)$$

where C is the molarity of NaCl and T is the temperature in K. All results of this study are presented in **Table I**. Also, to get the temperature dependence of the CO₂ diffusion coefficient, the Arrhenius law was used.

$$D = D_0 e^{-\frac{E_a}{RT}} \quad \text{or} \quad \ln D = \ln D_0 - \frac{E_a}{RT} \quad (7)$$

where D, D₀, E_a, R, and T are the diffusion coefficient, the pre-exponential factor, the activation energy, the gas constant, and the absolute temperature. **Figure 2** depicts the Arrhenius fits of the results of this study. By calculating their slope and putting it in equation (7), we can evaluate the activation energy for each of them. In the **Figure 2**, it is evident that the E_a value is almost constant up to 2 M. However, as the salinity increases, the value of E_a also increases, which means the diffusion mechanisms become harder and slower.

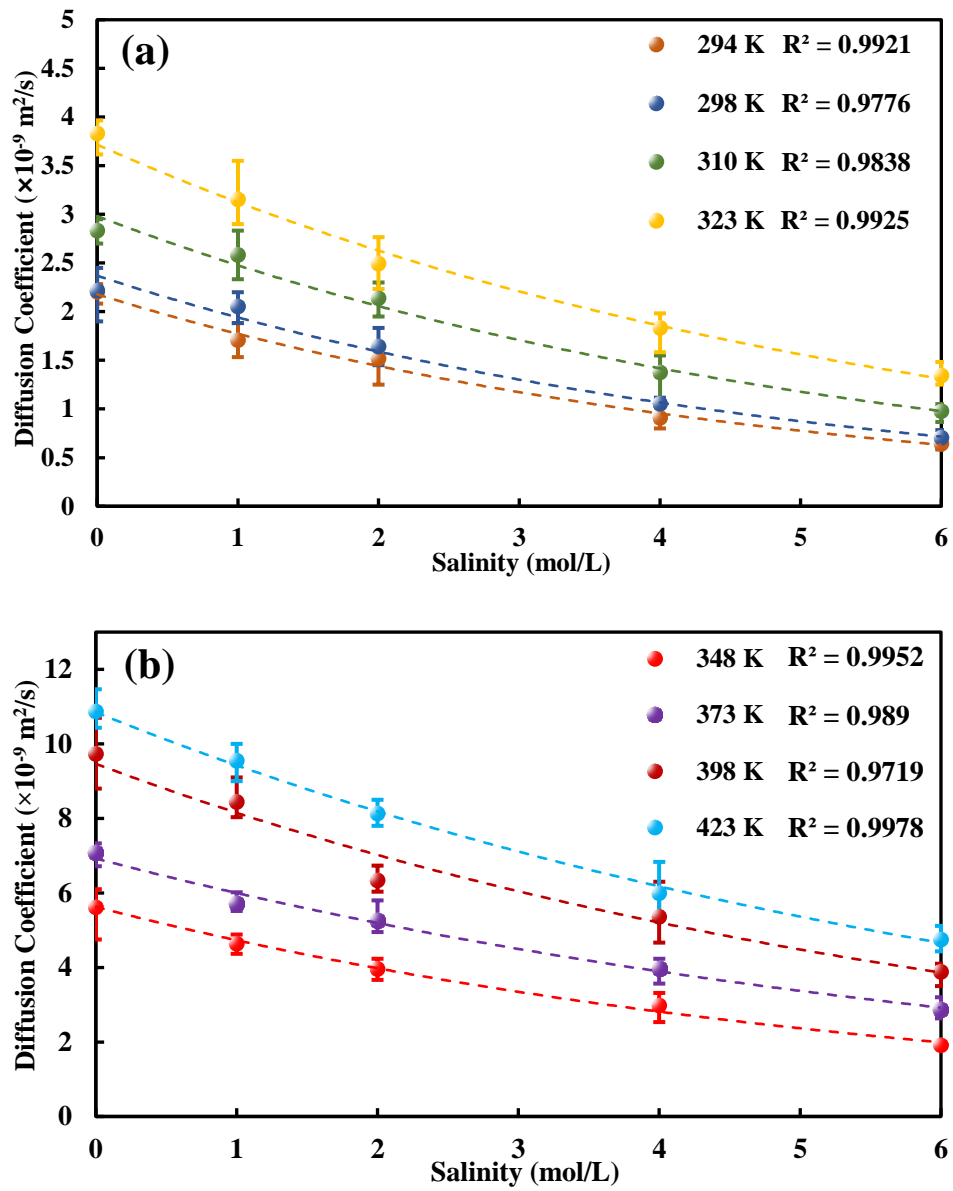


Figure 1- The CO₂ diffusion coefficient in 0-6 M NaCl solution at 10 MPa and temperatures of: a) 294-323 K b) 348-423 K.

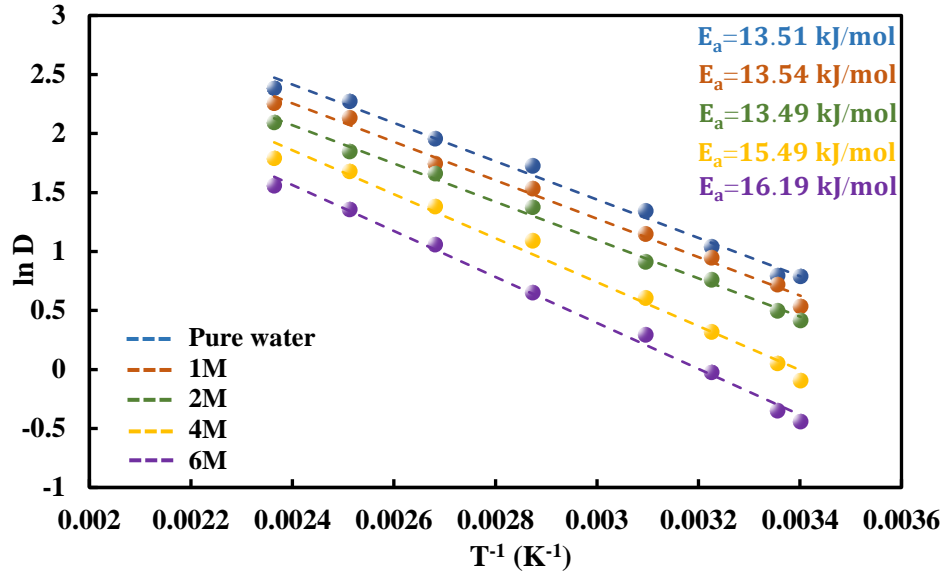


Figure 2- The Arrhenius plot of the CO₂ diffusion coefficient in water/brine for different NaCl concentrations.

Table 1- The results of the CO₂ diffusion coefficient in pure water/NaCl brine under various temperatures and pressures.

No.	Case Name	Solution ($\frac{\text{mol}}{\text{L}}$)	Temperature (K)	Pressure (MPa)	$D (\times 10^{-9} \frac{\text{m}^2}{\text{s}})$
1	T ₂₉₄ C ₀	Pure Water	294	100	2.2053
2	T ₂₉₄ C ₁	1 M NaCl	294	100	1.7082
3	T ₂₉₄ C ₂	2 M NaCl	294	100	1.5163
4	T ₂₉₄ C ₄	4 M NaCl	294	100	0.9109
5	T ₂₉₄ C ₆	6 M NaCl	294	100	0.6443
6	T ₂₉₈ C ₀	Pure Water	298	100	2.2167
7	T ₂₉₈ C ₁	1 M NaCl	298	100	2.0553
8	T ₂₉₈ C ₂	2 M NaCl	298	100	1.6443
9	T ₂₉₈ C ₄	4 M NaCl	298	100	1.0551
10	T ₂₉₈ C ₆	6 M NaCl	298	100	0.7055
11	T ₃₁₀ C ₀	Pure Water	310	100	2.8333
12	T ₃₁₀ C ₁	1 M NaCl	310	100	2.5831
13	T ₃₁₀ C ₂	2 M NaCl	310	100	2.1387
14	T ₃₁₀ C ₄	4 M NaCl	310	100	1.3777
15	T ₃₁₀ C ₆	6 M NaCl	310	100	0.9773
16	T ₃₁₀ C ₀ P ₂₀₀	Pure Water	310	200	2.7107
17	T ₃₁₀ C ₁ P ₂₀₀	1 M NaCl	310	200	2.5553
18	T ₃₁₀ C ₂ P ₂₀₀	2 M NaCl	310	200	2.1327
19	T ₃₁₀ C ₄ P ₂₀₀	4 M NaCl	310	200	1.4887
20	T ₃₁₀ C ₆ P ₂₀₀	6 M NaCl	310	200	0.9889
21	T ₃₁₀ C ₀ P ₃₀₀	Pure Water	310	300	2.8552

22	T ₃₁₀ C ₁ P ₃₀₀	1 M NaCl	310	300	2.3110
23	T ₃₁₀ C ₂ P ₃₀₀	2 M NaCl	310	300	2.0237
24	T ₃₁₀ C ₄ P ₃₀₀	4 M NaCl	310	300	1.4107
25	T ₃₁₀ C ₆ P ₃₀₀	6 M NaCl	310	300	0.8889
26	T ₃₂₃ C ₀	Pure Water	323	100	3.8327
27	T ₃₂₃ C ₁	1 M NaCl	323	100	3.1553
28	T ₃₂₃ C ₂	2 M NaCl	323	100	2.4940
29	T ₃₂₃ C ₄	4 M NaCl	323	100	1.8331
30	T ₃₂₃ C ₆	6 M NaCl	323	100	1.3443
31	T ₃₄₈ C ₀	Pure Water	348	100	5.6167
32	T ₃₄₈ C ₁	1 M NaCl	348	100	4.6385
33	T ₃₄₈ C ₂	2 M NaCl	348	100	3.9663
34	T ₃₄₈ C ₄	4 M NaCl	348	100	2.9831
35	T ₃₄₈ C ₆	6 M NaCl	348	100	1.9271
36	T ₃₄₈ C ₀ P ₂₀₀	Pure Water	348	200	5.4443
37	T ₃₄₈ C ₁ P ₂₀₀	1 M NaCl	348	200	4.1440
38	T ₃₄₈ C ₂ P ₂₀₀	2 M NaCl	348	200	3.9110
39	T ₃₄₈ C ₄ P ₂₀₀	4 M NaCl	348	200	2.6553
40	T ₃₄₈ C ₆ P ₂₀₀	6 M NaCl	348	200	1.9999
41	T ₃₄₈ C ₀ P ₃₀₀	Pure Water	348	300	5.2110
42	T ₃₄₈ C ₁ P ₃₀₀	1 M NaCl	348	300	4.4777
43	T ₃₄₈ C ₂ P ₃₀₀	2 M NaCl	348	300	4.0556
44	T ₃₄₈ C ₄ P ₃₀₀	4 M NaCl	348	300	2.6999
45	T ₃₄₈ C ₆ P ₃₀₀	6 M NaCl	348	300	1.7444
46	T ₃₇₃ C ₀	Pure Water	373	100	7.0820
47	T ₃₇₃ C ₁	1 M NaCl	373	100	5.7219
48	T ₃₇₃ C ₂	2 M NaCl	373	100	5.2610
49	T ₃₇₃ C ₄	4 M NaCl	373	100	3.9883
50	T ₃₇₃ C ₆	6 M NaCl	373	100	2.8830
51	T ₃₉₈ C ₀	Pure Water	398	100	9.7333
52	T ₃₉₈ C ₁	1 M NaCl	398	100	8.4443
53	T ₃₉₈ C ₂	2 M NaCl	398	100	6.3440
54	T ₃₉₈ C ₄	4 M NaCl	398	100	5.3663
55	T ₃₉₈ C ₆	6 M NaCl	398	100	3.8887
56	T ₄₂₃ C ₀	Pure Water	423	100	10.8773
57	T ₄₂₃ C ₁	1 M NaCl	423	100	9.5553
58	T ₄₂₃ C ₂	2 M NaCl	423	100	8.1333

59	$T_{423}C_4$	4 M NaCl	423	100	5.9997
60	$T_{423}C_6$	6 M NaCl	423	100	4.7497
61	$T_{423}C_0P_{200}$	Pure Water	423	200	11.2886
62	$T_{423}C_1P_{200}$	1 M NaCl	423	200	8.7773
63	$T_{423}C_2P_{200}$	2 M NaCl	423	200	8.4443
64	$T_{423}C_4P_{200}$	4 M NaCl	423	200	5.7775
65	$T_{423}C_6P_{200}$	6 M NaCl	423	200	4.9111
66	$T_{423}C_0P_{300}$	Pure Water	423	300	11.2775
67	$T_{423}C_1P_{300}$	1 M NaCl	423	300	9.0553
68	$T_{423}C_2P_{300}$	2 M NaCl	423	300	7.3442
69	$T_{423}C_4P_{300}$	4 M NaCl	423	300	6.1109
70	$T_{423}C_6P_{300}$	6 M NaCl	423	300	4.9889

To explore the reasons behind the behavior of the CO₂ diffusion coefficient in NaCl brine, we performed the RDF and H-bond analyses in each case separately. The RDF for Na-O_{H₂O}, Na-O_{CO₂}, Na-Cl and O_{CO₂}-H_{H₂O} in two temperatures of 294 K and 423 K are shown in **Figure 3** to **6**, respectively. The number of H-bonds between O_{CO₂}-H_{H₂O} and O_{H₂O}-H_{H₂O} are also illustrated in **Table 2**. First, we scrutinized the RDF figures and H-bond values to determine the impacts of the aforementioned parameters on intermolecular interactions between species. Then, we concluded the reason behinds the variation in CO₂ diffusion coefficient under different circumstances.

According to **Figure 3**, in general description, an increment in temperature reduces the magnitude of the first peak at each constant NaCl salinity concentration. Also, as the NaCl salinity rises, the height of the first peaks increases at relatively low temperatures, while at high temperatures (e.g., 423 K) go through a declining trend instead. In all cases, regardless of the salinity and temperature, the first hydration shell of Na⁺, identified by the first peak location of Na-O_{H₂O}, appears at 2.4 Å, in line with previous studies [32, 62-64]. The second hydration shell of Na⁺ is formed at approximately 4.5 Å, in which the height of the RDFs has a reverse order compared to the first peak values. It is worth noting that the second peak location of Na-O_{H₂O} has a negligible dependency on the temperature variation. The impacts of these changes can be explained by the dependency of intermolecular interactions of Na⁺ and water molecules on the concentration

and temperature. Regarding the impact of concentration, it is clear that the presence of more cations enhances the possibility of interactions with water molecules, resulting in more hydration shells. That is why a higher height is observed for more saline water. In respect of the temperature parameter, Na^+ ions are hydrated by water molecules, by which a strong attractive force is formed between water molecules and the surrounded ions. The temperature increase leads to Na^+ hydration shell size reduction, which triggers water molecules to decrease around the cations, facilitating the movement of Na^+ cations. In addition, the movement of water molecules increases because a rise in temperature intensifies repulsive forces among water molecules. This behavior that is shown by reduction in the height of RDFs with temperature increment is also confirmed by comparing the number of H-bond between water molecules provided in **Table 2**, which offers a decrease of intermolecular interactions among water molecules due to temperature increment. Nevertheless, in the case of the exception ($T= 423 \text{ K}$), there is no intense interaction between Na^+ and water molecules due to the higher NaCl salinity. In fact, the heating effect of the temperature may trigger spreading cations owing to a robust repulsive force among them, leading to a decrease in the possibility of the interactions with water molecules. That is why the height of the RDF is lower for the higher concentration at 423 K. Note that the RDFs of all cases are shown in **Figure S2**.

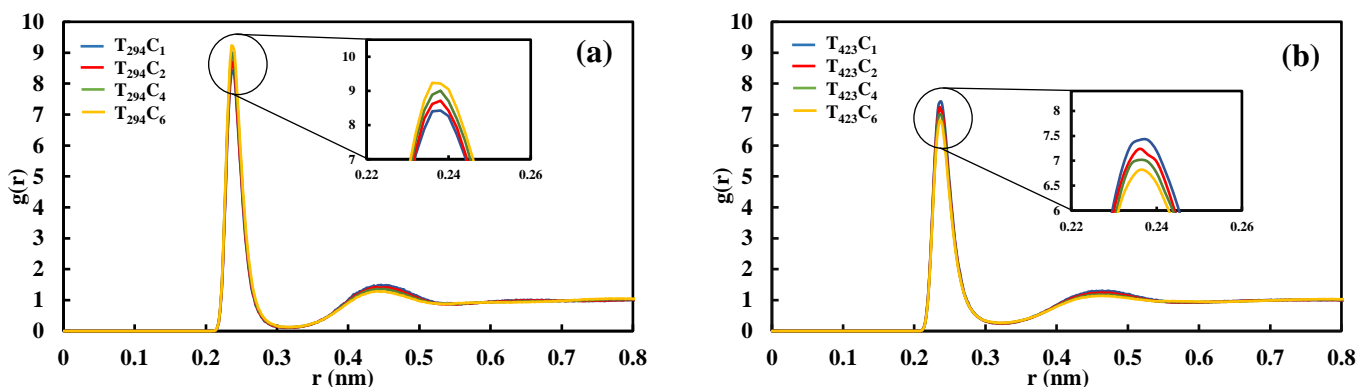


Figure 3- RDF curves of $\text{Na}-\text{O}_{\text{H}_2\text{O}}$ in various NaCl solutions at the temperatures of (a) 294 K, and (b) 423 K

Figure 4- demonstrates the RDF values of $\text{Na}-\text{O}_{\text{CO}_2}$ for two cases of 294 K and 423 K under various NaCl concentrations. RDFs of $\text{Na}-\text{O}_{\text{CO}_2}$ for the rest of cases are shown in **Figure S3**. As is shown, the RDF values experience a declining trend with temperature increment, in which the temperature changes have a relatively severe impact on the height of the RDFs, attributing to the higher NaCl concentrations.

Nevertheless, the distances between Na^+ and O_{CO_2} , identified by the first and second peak location of RDF, are fairly independent of temperature changes by taking the average distance of 2.58 Å and 5 Å, respectively. On the other hand, considering the salinity variation, the larger height of RDFs belongs to the higher NaCl concentrations at a constant temperature. Compared to the intermolecular interactions of Na^+ and water molecules, for all cases, rising the temperature decreases the affinity of Na^+ ions towards O_{CO_2} for each concentration, whereas the salinity increment enhances the intermolecular interplays between the cations and CO_2 molecules.

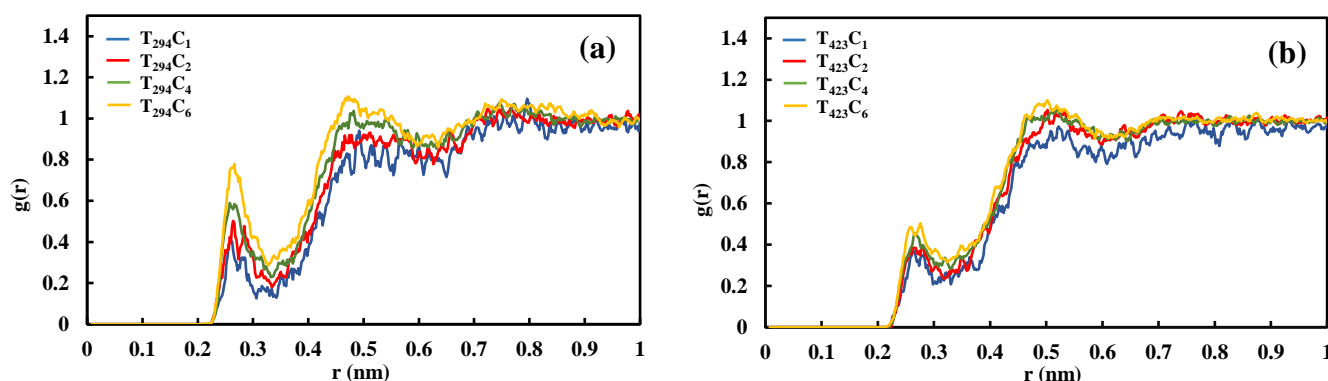


Figure 4-RDF curves of $\text{Na}-\text{O}_{\text{CO}_2}$ in various NaCl solutions at the temperatures of (a) 294 K, and (b) 423 K.

RDF curves for Na-Cl at temperatures of 294 K and 423 K are demonstrated in **Figure 5**. As is evident, although increasing temperature reduces the interaction intensity of $\text{Na}-\text{O}_{\text{H}_2\text{O}}$ and $\text{Na}-\text{O}_{\text{CO}_2}$, the intermolecular interactions of Na-Cl considerably enhance instead. Furthermore, the higher NaCl salinity concentration forms stronger interaction between Na-Cl. It can be inferred that at low temperatures, Na^+ cations are mainly hydrated by water molecules, and some of them lean towards CO_2 . However, the temperature increment reduces the interplays of water and CO_2 with Na^+ cations. Indeed, more interactions are created between Na-Cl (see **Figure S4** for the rest of the cases).

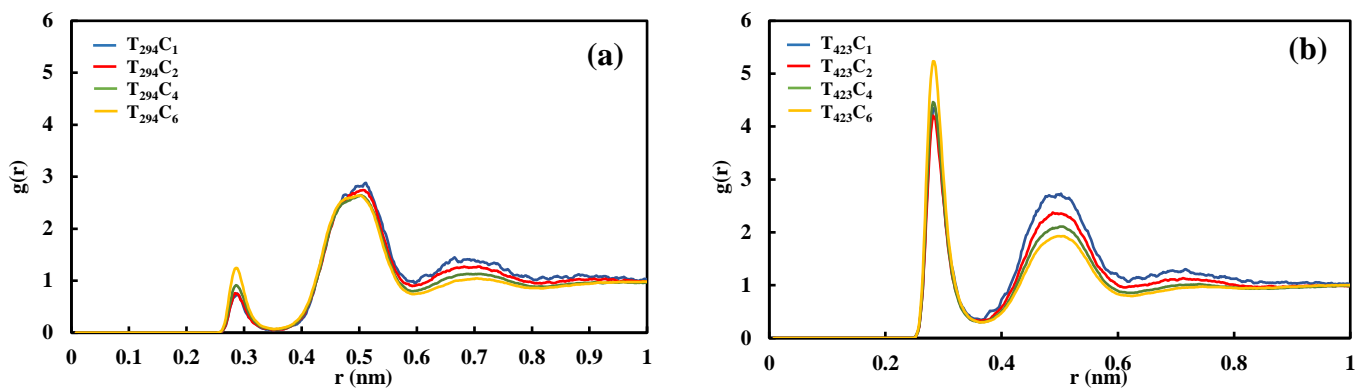


Figure 5- RDF curves of $Na-Cl$ in various NaCl solutions at the temperatures of a) 294 K, and b) 423 K

The RDFs for the pair of O_{CO_2} and H_{H_2O} in temperature of 294 K and 423 K are presented in **Figure 6-** RDF curves of $O_{CO_2}-H_{H_2O}$ in various aqueous solutions at the temperatures of (a) 294 K, and (b) 423 K.

(see **Figure S4** for the rest of the temperatures). It seems that an increase in temperature enhances the affinity of H_{H_2O} towards the O_{CO_2} since the slight jump in the first peak of RDFs at an average distance of 2 Å, which are linked to the presence of the H-bonds. The ascending trend of the number of H-bond between CO_2 and water molecules versus temperature increment proves the results of RDFs. According to **Table 2**, for the 1 M NaCl salinity concentration as an example, the number of H-bond between CO_2 and water molecules is 4.4352 and 6.1119 at 294 K and 423 K, respectively, indicating the stronger repulsive force among water molecules at elevated temperatures, which lead to improving the possibility of CO_2 surrounding by water molecules due to the temperature increase. Nevertheless, the second peak location of RDFs shifted to 3.9 Å from 3.4 Å at temperatures of 294 K and 423 K, respectively, identifying the weakening of the intermolecular interactions of the pairs at the larger distance. Furthermore, the presence of more Na^+ ions reinforces interactions of $O_{CO_2}-H_{H_2O}$ pairs. In more detail, when NaCl salinity concentration increases, more ionic hydration shells are also created. On the other hand, the solid electrostatic interactions between cations in the hydrated form with CO_2 leads to locating more water molecules close to the CO_2 . Subsequently, the intermolecular interplays between CO_2 and water molecules increase. **Table 2** also reveals the higher number of H-bond between $O_{CO_2}-H_{H_2O}$ pairs at more saline brine for all considered temperatures.

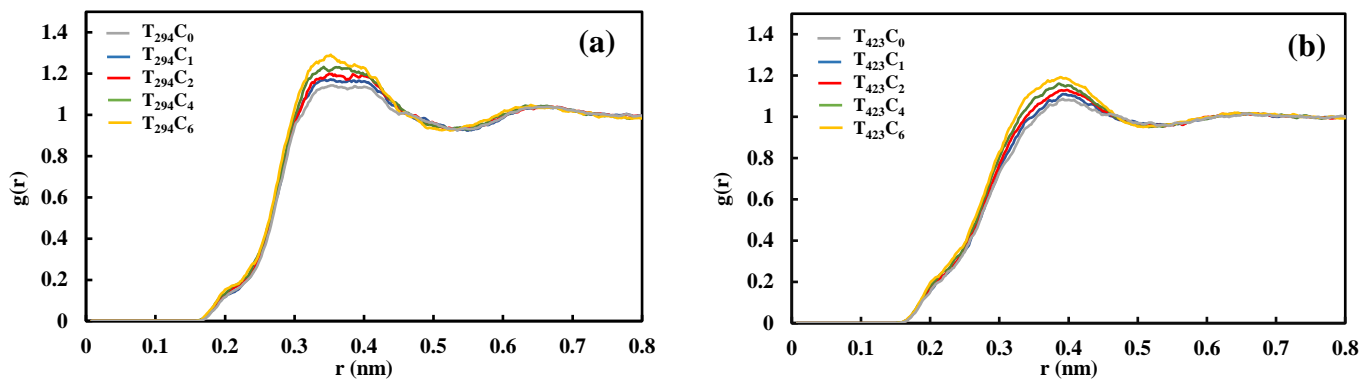


Figure 6- RDF curves of $O_{CO_2}-H_{H_2O}$ in various aqueous solutions at the temperatures of (a) 294 K, and (b) 423 K.

Table 2-The H-bonds values for $O_{CO_2}-H_{H_2O}$ and $O_{H_2O}-H_{H_2O}$.

		$O_{CO_2} - H_{H_2O}$				$O_{H_2O} - H_{H_2O}$			
Molarity (M)		1	2	4	6	1	2	4	6
Temperature (K)									
294		4.4352	4.6290	4.7613	4.8189	4798.8	4296.8	3380.3	2677.5
298		4.0551	4.6623	4.7672	4.9011	4730.7	4292.7	3386.8	2661.5
310		4.7107	4.8112	5.0119	5.0779	4687.4	4218.6	3330.1	2616.9
323		5.0839	5.2061	5.2235	5.2453	4613.6	4126.1	3306.2	2597.8
348		5.4535	5.4875	5.6154	5.7077	4498.5	3987.4	3191.7	2558.8
373		5.8182	5.9191	6.0083	6.0684	4308.9	3897.9	3089.6	2460.9
398		5.9445	6.0259	6.1114	6.2649	4145.9	3703.6	3030.1	2455.9
423		6.1119	6.1334	6.1909	6.2816	4001.8	3581.4	2952.3	2372.9

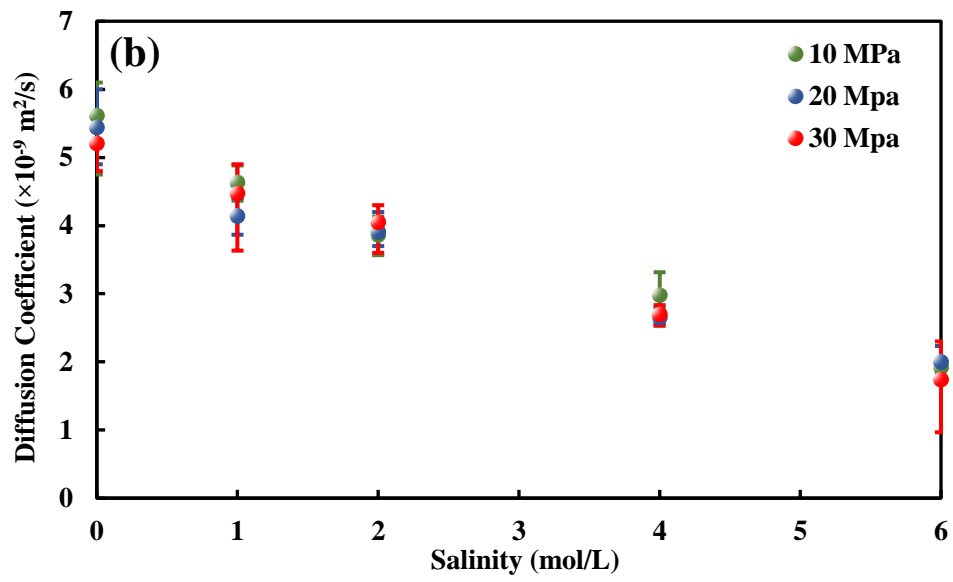
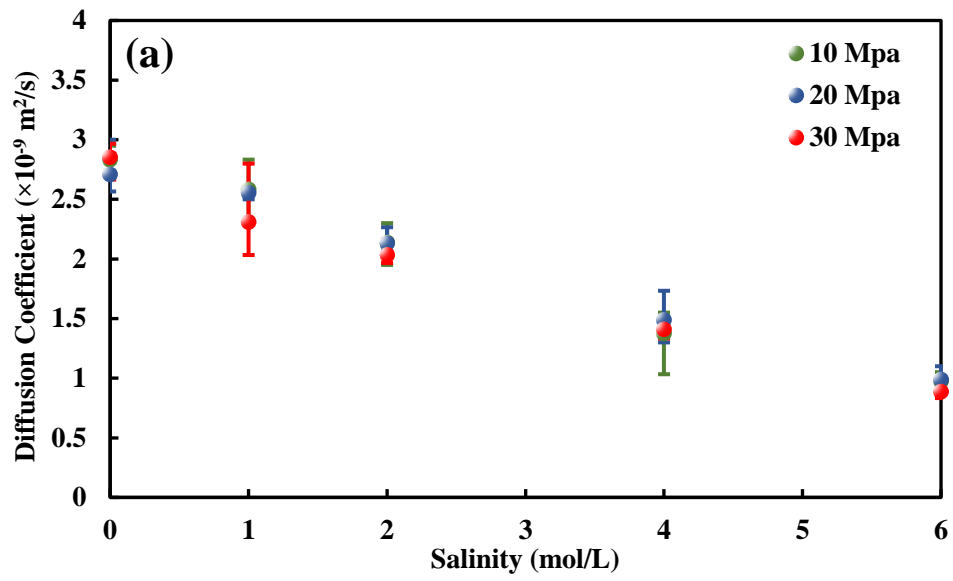
Overall, the increasing NaCl salinity not only enhances the affinity of Na^+ cations towards CO_2 molecules to form direct interactions but also locates more and more water molecules around themselves to form hydration shells. The formation of direct interactions and hydration shells impede the movement of CO_2 molecules. That is why the higher NaCl salinity restricts the freedom of CO_2 molecules, causing a decrease in the diffusion coefficient. Regarding the heat effect of the temperature, the rise in the CO_2 diffusion at elevated temperature originates from intensifying repulsive forces among Na^+ cations, resulting in lower intermolecular interaction with CO_2 molecules. Furthermore, since the hydration shells serve as a CO_2 movement barrier, a temperature rise reduces the size of hydration shells, providing more freedom for CO_2 molecules. There are the reasons behind higher CO_2 diffusion at elevated temperatures. It is worth

noting that although CO₂ molecules are more surrounded by water molecules separated from the cation's hydration shells due to the temperature increment, their interaction is not strong enough to restrict the freedom of CO₂ molecules as a result of lower CO₂ interactions with Na⁺ cations and decrease in size of hydration shells.

3.2. Pressure Effect on the CO₂ Diffusion Coefficient

Our investigation includes further analysis of pressure effects on the CO₂ diffusion coefficient, enabling us to obtain an in-depth understanding of critical parameters. According to the majority of previous studies, pressure does not significantly affect the diffusion coefficient, at least to a specific temperature and pressure [28, 65]. Nevertheless, Zhang et al. [16] claimed that the diffusion coefficient increases linearly with pressure, but this rise becomes smaller and smaller at some point. The results of Moulton et al. [36] demonstrated that the pressure effect on diffusion coefficient becomes more pronounced with increasing temperature, whereas before that, the change is negligible. In this study, simulations were repeated at 20 and 30 MPa at three levels of temperature: low (323 K), mediocre (373 K), and high (423 K). It was found that no substantial changes are present in the CO₂ diffusion coefficient under different pressures. According to **Figure 7**, it can be seen that there is neither a significant change in diffusion coefficients at various pressures nor does a remarkable trend indicate the coefficients are leaning toward higher or lower values with increasing pressure.

We also examined RDF values to corroborate our diffusion coefficient findings. These results can be seen in **Figures S6-S12**. In general, neither the peak values nor their distances change significantly at various pressures. For instance, the first and second peaks of Na-O_{H₂O} at 313 K and 10 MPa appear at 2.4 and 4.5 Å, respectively, and the same pattern is observed at 20 and 30 MPa, as well. Hence, the similarity in RDFs values of various pressures is aligned with the fact that pressure has no noticeable impact on the CO₂ diffusion coefficient.



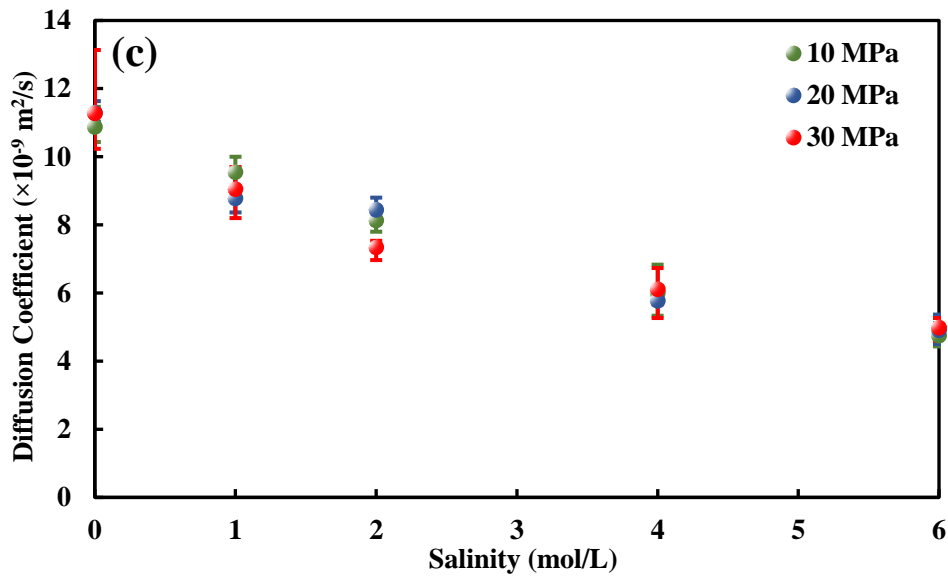


Figure 7- The CO₂ diffusion coefficient in 0-6 M NaCl solution under three different pressures of 10, 20, and 30 MPa and temperatures of (a) 310 K, (b) 348 K, and (c) 423 K.

3.3. Type of Salt Effect on the CO₂ Diffusion Coefficient

As is known, NaCl is the most common salt in aquifers, but other salt compositions may also be present. In fact, studies on the CO₂ diffusion coefficient in brine under the influence of various salt compositions have been limited to determining if any difference exists among them. Zhang et al. [16] considered four types of salts other than NaCl at 298 K and reported that the diffusion coefficient of CO₂ has the lowest and highest value in the presence of NaHCO₃ and CaCl₂, respectively. In 2015, Cadogan et al. [29] studied the CO₂ diffusion coefficients in brine containing NaCl, CaCl₂, and Na₂SO₄ separately. They found that NaCl has the smallest impact on the CO₂ diffusion coefficient compared to pure water, while Na₂SO₄ solution has the major contribution in changing the CO₂ diffusion coefficient.

Figure 8 displays the values of the CO₂ diffusion coefficient under the effect of different salts, including MgCl₂, CaCl₂, Na₂SO₄, and KCl. The simulations were carried out at 323 K and two levels of concentration (1 and 2 M). According to the results, CaCl₂ and KCl have the most and the least impact on the CO₂ diffusion coefficients compared to pure water, respectively. This indicates that analyzing water compositions regarding existent salts and their concentrations should be considered for the CCS process, particularly the CO₂ diffusion coefficient. Furthermore, the effect of different salts at higher concentrations on the CO₂ dissolution behavior is more prominent. **Table 3** lists the results of this section.

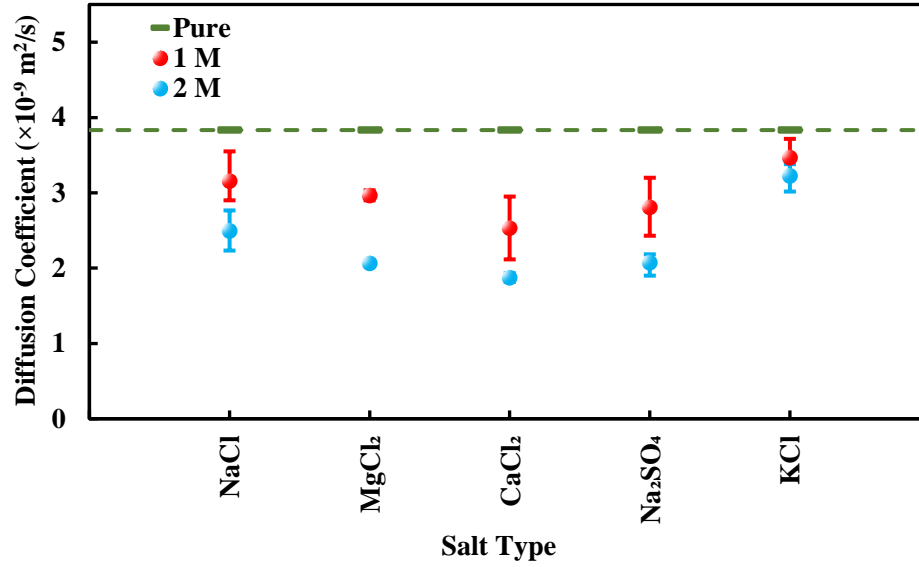


Figure 8- The CO₂ diffusion coefficient in brine in the presence of different salts under temperature of 323 K and pressure of 10 MPa.

Table 3- The results of CO₂ diffusion coefficient in various brine solutions.

No.	Case Name	Solution ($\frac{\text{mol}}{\text{L}}$)	Temperature (K)	Pressure (MPa)	D ($\times 10^{-9} \frac{\text{m}^2}{\text{s}}$)
1	T ₃₂₃ C ₁ S _{MgCl₂}	1 M MgCl ₂	323	100	2.9665
2	T ₃₂₃ C ₂ S _{MgCl₂}	2 M MgCl ₂	323	100	2.0663
3	T ₃₂₃ C ₁ S _{CaCl₂}	1 M CaCl ₂	323	100	2.5330
4	T ₃₂₃ C ₂ S _{CaCl₂}	2 M CaCl ₂	323	100	1.8747
5	T ₃₂₃ C ₁ S _{Na₂SO₄}	1 M Na ₂ SO ₄	323	100	2.8100
6	T ₃₂₃ C ₂ S _{Na₂SO₄}	2 M Na ₂ SO ₄	323	100	2.0721
7	T ₃₂₃ C ₁ S _{KCl}	1 M KCl	323	100	3.4660
8	T ₃₂₃ C ₂ S _{KCl}	2 M KCl	323	100	3.2266

We analyzed the RDF values for the involved components to obtain the relationship between the salt composition and the CO₂ diffusion coefficient. Generally, it can be said that due to the difference in the nature of salt components, their intermolecular interactions with water and CO₂ are varied. That is why no straightforward relationship is defined for the salt compositions and the CO₂ diffusion coefficient. Nevertheless, there are some valuable points regarding the mechanisms of salts on changing the CO₂ diffusion that should be discussed. **Figure 9a** shows that the first hydration shell of Na⁺, Mg²⁺, Ca²⁺, and K⁺ are located at 2.4, 2.1, 2.4, and 2.8 Å, respectively, which is consistent with previous studies [45, 66]. As is

clear, the maximum intensity of the cation interaction with water molecules belongs to Mg^{2+} , Ca^{2+} , Na^+ of NaCl , K^+ , and Na^+ of Na_2SO_4 , respectively. While the higher tendency of the cation interaction with water molecules, the less intensity of the cation interaction with CO_2 will result, except Na^+ of Na_2SO_4 (see **Figure 9b**). On the other hand, comparing the RDFs of cations with anions reveals that most cations in Na_2SO_4 solutions tend to interact with anions rather than water or CO_2 molecules, as shown in **Figure 10a**. In other words, the strong interaction between Na^+ and SO_4^{2-} explains the low hydration tendency of Na^+ ions and their less affinity towards CO_2 molecules. The intense interaction between cations and anions is also evident in MgCl_2 . This also can justify the low interaction of Mg^{2+} with CO_2 molecules. **Figure 10b** illustrates RDFs of $\text{H}_{\text{H}_2\text{O}}\text{-O}_{\text{H}_2\text{O}}$ that have the same trends for all cases. However, in the case of Na_2SO_4 , since ionic compositions have a higher tendency towards each other, water molecules also have more freedom to interact with CO_2 . According to the intermolecular interactions of cations, it can be concluded that salts can reduce the movement of CO_2 molecules in saline brine following three possible mechanisms of the direct interaction of cations with CO_2 , formation of cations' hydration, and aggregation of ionic components. In further detail, monovalent cations with low hydration enthalpy, which have no robust tendency towards water, can interplay with CO_2 molecules directly, leading to the interruption of CO_2 freedom (e.g., KCl). Cations with a strong attraction towards the water molecules can form hydration shells, acting as a barrier for the movement of CO_2 (e.g., MgCl_2). In addition, ionic compositions with the potential of aggregation formation (e.g., Na_2SO_4) can restrict the CO_2 diffusion in saline brine. Also, the formed ionic cluster occupies a large amount of space, causing less volume available for CO_2 molecules. Note that brine like MgCl_2 may influence the CO_2 diffusion coefficient by following two mechanisms. **Figure 11** illustrates the final snapshots of the simulation box containing different salts.

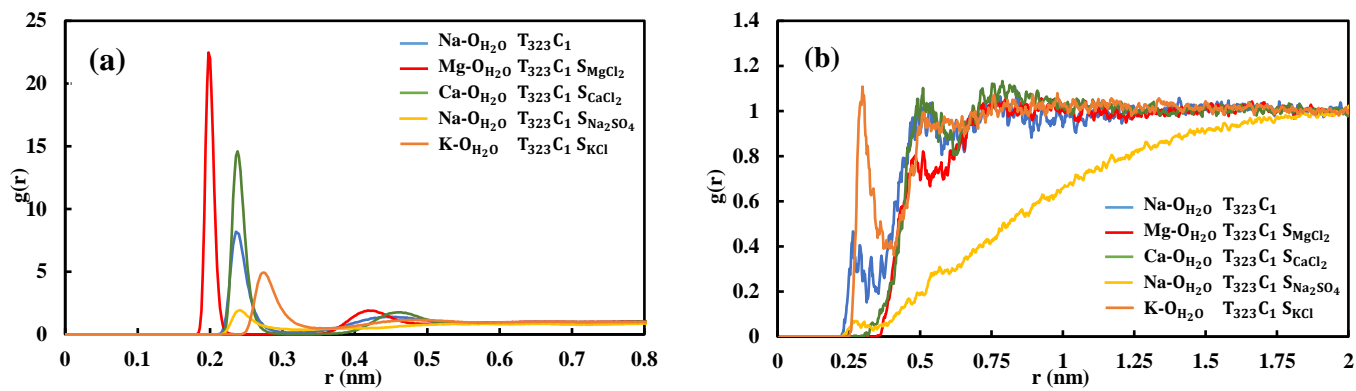


Figure 9- The RDF values between cations and (a) O_{H_2O} and (b) O_{CO_2} in various saline solutions at the temperatures 323 K and 1 M concentration.

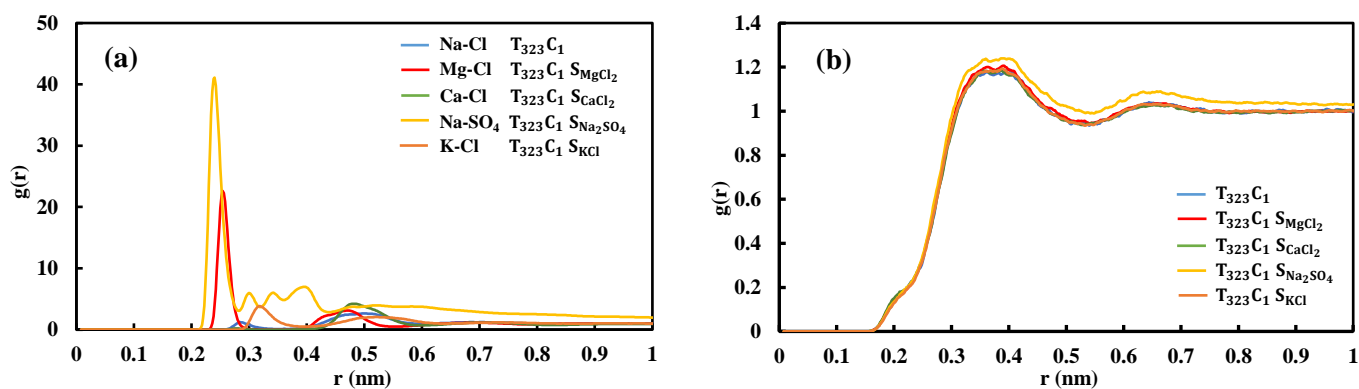


Figure 10- The RDF values between (a) cations-anions and (b) H_{H_2O} - O_{H_2O} in various saline solutions at the temperatures 323 K and 1 M concentration.

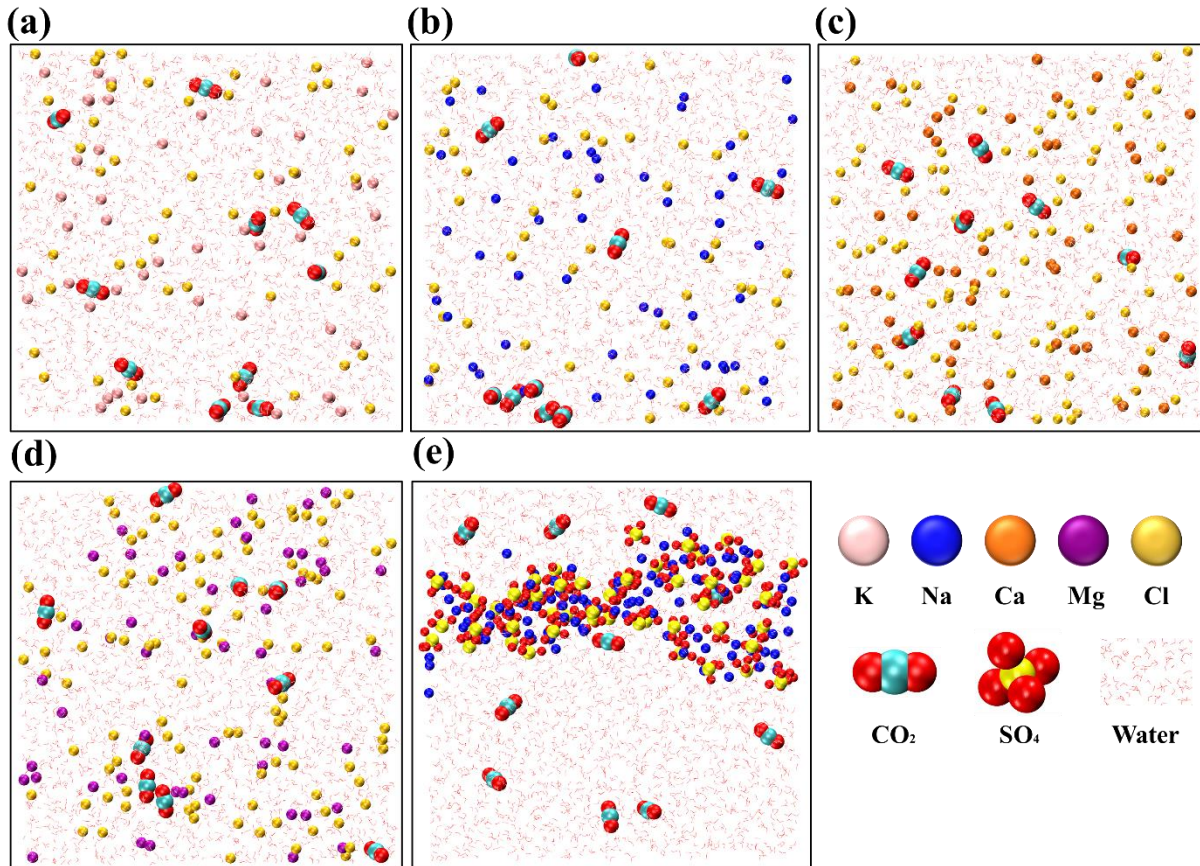


Figure 11- Final Snapshots of simulation systems containing solution with the name of (a) $T_{323}C_1S_{KCl}$, (b) $T_{323}C_1S_{NaCl}$, (c) $T_{323}C_1S_{CaCl_2}$, (d) $T_{323}C_1S_{MgCl_2}$, and (e) $T_{323}C_1S_{Na_2SO_4}$. As is clear, the tendency of ionic compositions to create aggregations is in order of (e)> (d)> (c)> (b)> (a).

3.4. CO₂ Dissolution Behavior

In order to get further insight into the difference between considering and ignoring the change of CO₂ diffusion coefficient in CO₂ dissolution behavior, we considered the cases of CO₂ diffusion in NaCl brine at 323 K for direct numerical simulation. **Figure 12** illustrates the averaged dissolved CO₂ (normalized by maximum solubility) and CO₂ dissolution flux for each case (dashed curves are those without considering the salt effect, and their names include * at the end). The lack of consideration of diffusion coefficient changes in 1M NaCl solution results in a wrong evaluation of dissolved CO₂ and an overestimation of dissolution flux. Furthermore, without considering the actual CO₂ diffusion coefficient at higher salinities, both dissolved CO₂ and dissolution flux would seem to be excessively high at higher salinities (e.g., 4M). Considering the initial stage of the CO₂ dissolution process (beginning of the curves of dissolved CO₂ in **Figure 12a**), all cases based on the pure water CO₂ diffusion coefficient show a higher amount of dissolved

CO₂, suggesting the overestimation of the diffusion mechanism strength. It can be inferred that predicting CO₂ dissolution process parameters without considering the correct diffusion coefficient results in massive errors. **Figure 13** displays the dissolved CO₂ pattern for cases T₃₂₃C₀, T₃₂₃C₁, T₃₂₃C₁^{*}, T₃₂₃C₄, and T₃₂₃C₄^{*}. Even if we disregard the differences in dissolved CO₂ and dissolution flux, time differences can significantly impact the long-term CO₂ sequestration planning. In addition, these behaviors are more pronounced at higher temperatures. Considering the same salinity, if pure water CO₂ diffusion is used instead of the real brine diffusion coefficient, then the damping capability of the system for gravitational instabilities increases unrealistically. Therefore, the relative importance of the convective to diffusive mechanism decreases, and a delay in dissolution regimes changes is observed. It should be noted that the transition times between dissolution regimes is controlled by not only diffusion coefficient but also density difference, which is a critical factor in the solubility process. That is why cases with 4 M salinity show the latest transition times. Since the solubility values are the lowest in these cases, the density difference, considered the driving force for the convective flow, would be the lowest. At all, in spite of the minimum diffusion coefficient for assessed cases, the density difference has more control on the system, and it increases the transition times.

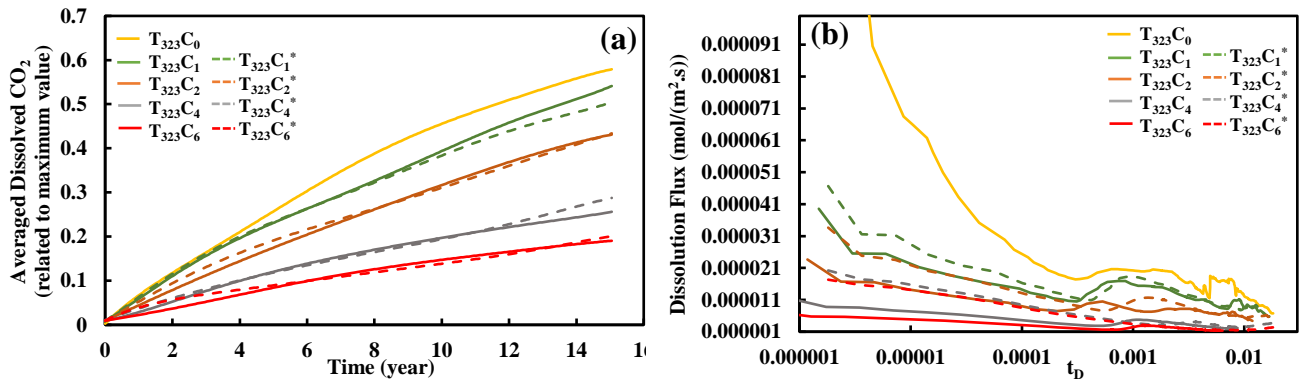


Figure 12- (a) Averaged dissolved CO₂ and (b) dissolution flux for cases at 323 K.

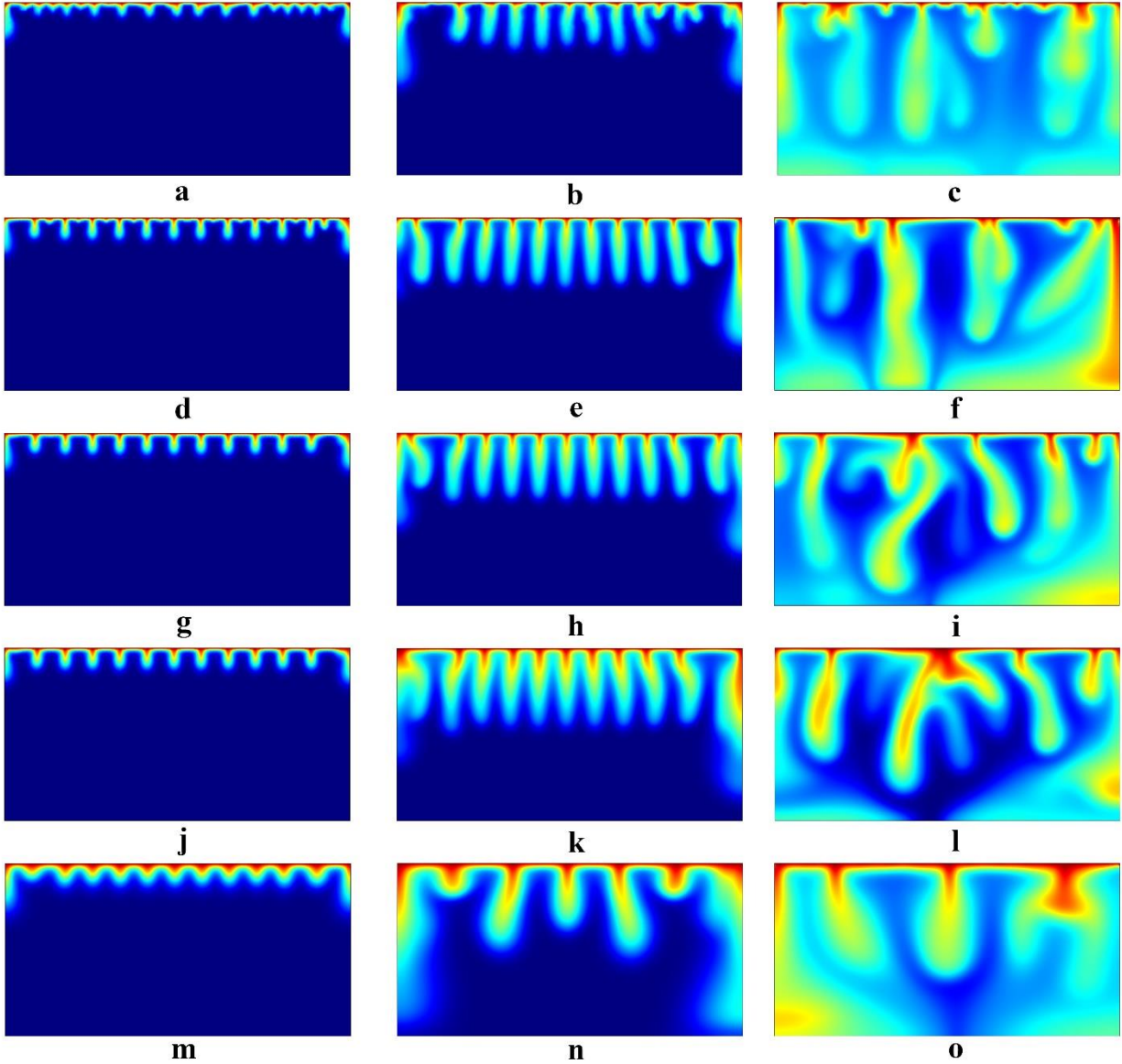


Figure 13- Dissolved CO₂ patterns for cases T₃₂₃C₀ (first row), T₃₂₃C₁ (second row), T₃₂₃C₁^{*} (third row), T₃₂₃C₄ (fourth row), and T₃₂₃C₄^{*} (fifth row): a) T₃₂₃C₀ at onset of convection (0.25 year), b) T₃₂₃C₀ in the quasi-steady state (0.4 years), c) T₃₂₃C₀ at the onset of shut-down (7.5 years), d) T₃₂₃C₁ at onset of convection (0.31 year), e) T₃₂₃C₁ in the quasi-steady state (0.6 years), f) T₃₂₃C₁ at the onset of shut-down (9 years), g) T₃₂₃C₁^{*} at onset of convection (0.35 years), h) T₃₂₃C₁^{*} in the quasi-steady state (0.65 years), i) T₃₂₃C₁^{*} at the onset of shut-down (10.25 years), j) T₃₂₃C₄ at onset of convection (0.8 year), k) T₃₂₃C₄ in the quasi-steady state (1.6 years), l) T₃₂₃C₄ at the onset of shut-down (20.4 years), m) T₃₂₃C₄^{*} at onset of convection (1.4 years), n) T₃₂₃C₄^{*} in the quasi-steady state (2.4 years), o) T₃₂₃C₄^{*} at the onset of shut-down (21.8 years).

4. Conclusions

In this research, a comprehensive study on the CO₂ diffusion coefficient in water/brine under a wide range of temperature (294-423 K) and NaCl concentration (1-6 M) was performed through MD simulation, and a thorough data set was provided. In addition, the role of pressure variation and composition of salts on the

CO₂ diffusion coefficient changes were examined. Finally, the direct numerical simulation was employed to highlight differences in the CO₂ dissolution process between assuming the CO₂ diffusion coefficient in brine rather than pure water. The highlight important points of this research are as follows:

- 1- The CO₂ diffusion coefficient decreases monotonically with increasing NaCl salinity concentration at a constant temperature, while the diffusion coefficients go through the trend of rising as the temperature increases for each concentration. The formation of Na⁺ cation hydration shells, which act as an obstacle to CO₂ movement, is the primary reason for the diffusion coefficient reduction. Since fewer water molecules are present in the hydration shell of cations at higher temperatures, a higher diffusion coefficient also results. Also, for predicting the CO₂ diffusion coefficient, a new correlation was proposed in terms of temperature and NaCl salinity concentration with the relative accuracy of $R^2 = 0.988$.
- 2- Pressure variation has a negligible influence on the CO₂ diffusion coefficient in water/saline brine under different temperature and salinity concentrations. While salinity compositions change the CO₂ diffusion coefficient, in which CaCl₂ and KCl have the highest and lowest impact on the CO₂ diffusion coefficient reduction, respectively. It is worth noting that there exists not an accurate relationship between the type of salt and the CO₂ diffusion coefficient decrease.
- 3- Salts can lessen the value of the CO₂ diffusion coefficient following three possible mechanisms, including restriction of the CO₂ movement via direct interplays of CO₂ molecules and cations, interrupting the CO₂ freedom through the formation of cations' hydration, and reducing the available space and creation of CO₂ movement barrier by the appearance of ionic aggregations.
- 4- According to direct numerical simulation results, the lack of data for the CO₂ diffusion coefficient in brine results in false predictions and substantial errors in calculating the CO₂ dissolution behavior. This includes overestimating or underestimating dissolved CO₂ dissolution flux and the onset of different CO₂ dissolution regimes.

Since there is lacking data for the CO₂ diffusion coefficient in water/saline brine under a real geological condition, we hope that our research paves the way for future research pertaining to CO₂ sequestration in saline aquifers so as to have long-term and safe underground CO₂ storage.

References

1. Hu, H., Y. Xing, and X. Li, *Self-diffusivity, M–S and Fick diffusivity of CO₂ in Na-clay: The influences of concentration and temperature*. Scientific reports, 2017. **7**(1): p. 1-10.
2. Li, D. and X. Jiang, *Numerical investigation of convective mixing in impure CO₂ geological storage into deep saline aquifers*. International Journal of Greenhouse Gas Control, 2020. **96**: p. 103015.
3. Gholami, Y., et al., *Suggesting a numerical pressure-decay method for determining CO₂ diffusion coefficient in water*. Journal of Molecular Liquids, 2015. **211**: p. 31-39.
4. Raad, S.M.J. and H. Hassanzadeh, *Does impure CO₂ impede or accelerate the onset of convective mixing in geological storage?* International Journal of Greenhouse Gas Control, 2016. **54**: p. 250-257.
5. Alcalde, J., et al., *Estimating geological CO₂ storage security to deliver on climate mitigation*. Nature communications, 2018. **9**(1): p. 1-13.
6. Li, D., et al., *Numerical analyses of the effects of nitrogen on the dissolution trapping mechanism of carbon dioxide geological storage*. Computers & Fluids, 2015. **114**: p. 1-11.
7. Li, D. and X. Jiang, *Numerical investigation of the partitioning phenomenon of carbon dioxide and multiple impurities in deep saline aquifers*. Applied Energy, 2017. **185**: p. 1411-1423.
8. Raad, S.M.J. and H. Hassanzadeh, *Does impure CO₂ impede or accelerate the onset of convective mixing in geological storage*. International Journal of Greenhouse Gas Control, 2016. **54**: p. 250-257.
9. Mojtaba, S., et al., *Experimental study of density-driven convection effects on CO₂ dissolution rate in formation water for geological storage*. Journal of Natural Gas Science and Engineering, 2014. **21**: p. 600-607.

10. Thomas, C., S. Dehaeck, and A. De Wit, *Convective dissolution of CO₂ in water and salt solutions*. International Journal of Greenhouse Gas Control, 2018. **72**: p. 105-116.
11. Mahmoodpour, S., et al., *Effect of brine composition on the onset of convection during CO₂ dissolution in brine*. Computers & Geosciences, 2019. **124**: p. 1-13.
12. Omrani, S., et al., *Diffusion coefficients of CO₂-SO₂-water and CO₂-N₂-water systems and their impact on the CO₂ sequestration process: Molecular dynamics and dissolution process simulations*. Greenhouse Gases: Science and Technology, 2021.
13. Yang, C. and Y. Gu, *Accelerated mass transfer of CO₂ in reservoir brine due to density-driven natural convection at high pressures and elevated temperatures*. Industrial & engineering chemistry research, 2006. **45**(8): p. 2430-2436.
14. Farajzadeh, R., P.L. Zitha, and J. Bruining, *Enhanced mass transfer of CO₂ into water: experiment and modeling*. Industrial & Engineering Chemistry Research, 2009. **48**(13): p. 6423-6431.
15. Sell, A., et al., *Measurement of CO₂ diffusivity for carbon sequestration: A microfluidic approach for reservoir-specific analysis*. Environmental science & technology, 2013. **47**(1): p. 71-78.
16. Zhang, W., et al., *The modeling and experimental studies on the diffusion coefficient of CO₂ in saline water*. Journal of CO₂ Utilization, 2015. **11**: p. 49-53.
17. Belgodere, C., et al., *Experimental determination of CO₂ diffusion coefficient in aqueous solutions under pressure at room temperature via Raman spectroscopy: impact of salinity (NaCl)*. Journal of Raman Spectroscopy, 2015. **46**(10): p. 1025-1032.
18. Raad, S.M.J., R. Azin, and S. Osfour, *Measurement of CO₂ diffusivity in synthetic and saline aquifer solutions at reservoir conditions: the role of ion interactions*. Heat and Mass Transfer, 2015. **51**(11): p. 1587-1595.
19. SCRIVEN II, L.E., *Interfacial resistance in gas absorption*. 1956: University of Delaware.
20. Woods, D.R., *Mass Transfer Between a Liquid Jet and a Counter-current Gas Stream*. 1961: University of Wisconsin--Madison.

21. Tang, Y. and D. Himmelblau, *Effect of solute concentration on the diffusivity of carbon dioxide in water*. Chemical Engineering Science, 1965. **20**(1): p. 7-14.
22. Vivian, J.E. and C.J. King, *Diffusivities of slightly soluble gases in water*. AIChE Journal, 1964. **10**(2): p. 220-221.
23. Unver, A. and D. Himmelblau, *Diffusion Coefficients of CO₂, C₂H₄, C₃H₆ and C₄H₈ in Water from 6 to 65 C*. Journal of Chemical & Engineering Data, 1964. **9**(3): p. 428-431.
24. Thomas, W. and M. Adams, *Measurement of the diffusion coefficients of carbon dioxide and nitrous oxide in water and aqueous solutions of glycerol*. Transactions of the Faraday Society, 1965. **61**: p. 668-673.
25. Ferrell, R.T. and D.M. Himmelblau, *Diffusion coefficients of nitrogen and oxygen in water*. Journal of chemical and engineering data, 1967. **12**(1): p. 111-115.
26. Tamimi, A., E.B. Rinker, and O.C. Sandall, *Diffusion coefficients for hydrogen sulfide, carbon dioxide, and nitrous oxide in water over the temperature range 293-368 K*. Journal of Chemical and Engineering data, 1994. **39**(2): p. 330-332.
27. Hirai, S., et al., *Measurement of CO₂ diffusion coefficient and application of LIF in pressurized water*. Energy, 1997. **22**(2-3): p. 363-367.
28. Cadogan, S.P., G.C. Maitland, and J.M. Trusler, *Diffusion coefficients of CO₂ and N₂ in water at temperatures between 298.15 K and 423.15 K at pressures up to 45 MPa*. Journal of Chemical & Engineering Data, 2014. **59**(2): p. 519-525.
29. Cadogan, S.P., et al., *Diffusion coefficients of carbon dioxide in brines measured using ¹³C pulsed-field gradient nuclear magnetic resonance*. Journal of Chemical & Engineering Data, 2015. **60**(1): p. 181-184.
30. Yuan, C., et al., *CO₂/N₂-switchable sol-gel transition based on NaDC/NaCl solution: Experiments and molecular dynamics simulations*. Journal of Molecular Liquids, 2021. **325**: p. 115193.
31. dos Santos, T.J., F.W. Tavares, and C.R. Abreu, *Fick diffusion coefficients via molecular dynamics: An alternative approach in the Fourier domain*. Journal of Molecular Liquids, 2021. **329**: p. 115460.

32. Ghasemi, M. and M. Sharifi, *Effects of layer-charge distribution on swelling behavior of mixed-layer illite-montmorillonite clays: A molecular dynamics simulation study*. Journal of Molecular Liquids, 2021. **335**: p. 116188.
33. Tsimpanogiannis, I.N., et al., *Self-diffusion coefficient of bulk and confined water: a critical review of classical molecular simulation studies*. Molecular Simulation, 2019. **45**(4-5): p. 425-453.
34. Jamali, S.H., et al., *Finite-size effects of binary mutual diffusion coefficients from molecular dynamics*. Journal of chemical theory and computation, 2018. **14**(5): p. 2667-2677.
35. Garcia-Rates, M., et al., *Molecular modeling of diffusion coefficient and ionic conductivity of CO₂ in aqueous ionic solutions*. The Journal of Physical Chemistry B, 2012. **116**(9): p. 2787-2800.
36. Moulτος, O.A., et al., *Atomistic molecular dynamics simulations of CO₂ diffusivity in H₂O for a wide range of temperatures and pressures*. The Journal of Physical Chemistry B, 2014. **118**(20): p. 5532-5541.
37. Yang, H., et al., *A reverse nonequilibrium molecular dynamics method for calculating the mutual diffusion coefficient for binary fluids*. Chemical Engineering Science, 2015. **130**: p. 1-7.
38. Stephan, S., et al., *MolMod—an open access database of force fields for molecular simulations of fluids*. Molecular Simulation, 2019. **45**(10): p. 806-814.
39. Wheeler, D.R. and J. Newman, *Molecular dynamics simulations of multicomponent diffusion. 2. Nonequilibrium method*. The Journal of Physical Chemistry B, 2004. **108**(47): p. 18362-18367.
40. Mutoru, J.W., A. Leahy-Dios, and A. Firoozabadi, *Modeling infinite dilution and Fickian diffusion coefficients of carbon dioxide in water*. AIChE journal, 2011. **57**(6): p. 1617-1627.
41. Potoff, J.J. and J.I. Siepmann, *Vapor–liquid equilibria of mixtures containing alkanes, carbon dioxide, and nitrogen*. AIChE journal, 2001. **47**(7): p. 1676-1682.
42. Perez-Blanco, M.E. and E.J. Maginn, *Molecular dynamics simulations of CO₂ at an ionic liquid interface: Adsorption, ordering, and interfacial crossing*. The Journal of Physical Chemistry B, 2010. **114**(36): p. 11827-11837.

43. Harris, J.G. and K.H. Yung, *Carbon dioxide's liquid-vapor coexistence curve and critical properties as predicted by a simple molecular model*. The Journal of Physical Chemistry, 1995. **99**(31): p. 12021-12024.
44. Smith, D.E. and L.X. Dang, *Computer simulations of NaCl association in polarizable water*. The Journal of Chemical Physics, 1994. **100**(5): p. 3757-3766.
45. Joung, I.S. and T.E. Cheatham III, *Determination of alkali and halide monovalent ion parameters for use in explicitly solvated biomolecular simulations*. The journal of physical chemistry B, 2008. **112**(30): p. 9020-9041.
46. Berendsen, H., J. Grigera, and T. Straatsma, *The missing term in effective pair potentials*. Journal of Physical Chemistry, 1987. **91**(24): p. 6269-6271.
47. Mirzaie, M. and A. Tatar, *Modeling of interfacial tension in binary mixtures of CH₄, CO₂, and N₂-alkanes using gene expression programming and equation of state*. Journal of Molecular Liquids, 2020. **320**: p. 114454.
48. Berendsen, H.J., D. van der Spoel, and R. van Drunen, *GROMACS: a message-passing parallel molecular dynamics implementation*. Computer physics communications, 1995. **91**(1-3): p. 43-56.
49. Nosé, S., *A molecular dynamics method for simulations in the canonical ensemble*. Molecular physics, 1984. **52**(2): p. 255-268.
50. Hoover, W.G., *Canonical dynamics: Equilibrium phase-space distributions*. Physical review A, 1985. **31**(3): p. 1695.
51. Parrinello, M. and A. Rahman, *Polymorphic transitions in single crystals: A new molecular dynamics method*. Journal of Applied physics, 1981. **52**(12): p. 7182-7190.
52. Hess, B., et al., *LINCS: a linear constraint solver for molecular simulations*. Journal of computational chemistry, 1997. **18**(12): p. 1463-1472.
53. Allen, M.P. and D.J. Tildesley, *Computer simulation of liquids*. 2017: Oxford university press.
54. Celebi, A.T., et al., *Finite-size effects of diffusion coefficients computed from molecular dynamics: a review of what we have learned so far*. Molecular Simulation, 2020: p. 1-15.

55. Dünweg, B. and K. Kremer, *Molecular dynamics simulation of a polymer chain in solution*. The Journal of chemical physics, 1993. **99**(9): p. 6983-6997.
56. Duan, Z. and R. Sun, *An improved model calculating CO₂ solubility in pure water and aqueous NaCl solutions from 273 to 533 K and from 0 to 2000 bar*. Chemical geology, 2003. **193**(3-4): p. 257-271.
57. Garcia, J.E., *Density of aqueous solutions of CO₂*. 2001, Lawrence Berkeley National Lab.(LBNL), Berkeley, CA (United States).
58. Mao, S. and Z. Duan, *The P, V, T, x properties of binary aqueous chloride solutions up to T= 573 K and 100 MPa*. The Journal of Chemical Thermodynamics, 2008. **40**(7): p. 1046-1063.
59. Mao, S. and Z. Duan, *The viscosity of aqueous alkali-chloride solutions up to 623 K, 1,000 bar, and high ionic strength*. International Journal of Thermophysics, 2009. **30**(5): p. 1510-1523.
60. Mahmoodpour, S., et al., *Convective dissolution of carbon dioxide in deep saline aquifers: Insights from engineering a high-pressure porous visual cell*. Physical Review Applied, 2019. **12**(3): p. 034016.
61. Mahmoodpour, S., B. Rostami, and H. Emami-Meybodi, *Onset of convection controlled by N₂ impurity during CO₂ storage in saline aquifers*. International Journal of Greenhouse Gas Control, 2018. **79**: p. 234-247.
62. Denis, J., et al., *Influence of potassium concentration on the swelling and compaction of mixed (Na, K) ion-exchanged montmorillonite*. Clay Minerals, 1991. **26**(2): p. 255-268.
63. Rahromostaqim, M. and M. Sahimi, *Molecular dynamics simulation of hydration and swelling of mixed-layer clays*. The Journal of Physical Chemistry C, 2018. **122**(26): p. 14631-14639.
64. Rahromostaqim, M. and M. Sahimi, *Molecular dynamics simulation of hydration and swelling of mixed-layer clays in the presence of carbon dioxide*. The Journal of Physical Chemistry C, 2019. **123**(7): p. 4243-4255.

65. Tsimpanogiannis, I.N., et al., *Engineering Model for Predicting the Intradiffusion Coefficients of Hydrogen and Oxygen in Vapor, Liquid, and Supercritical Water based on Molecular Dynamics Simulations*. Journal of Chemical & Engineering Data, 2021.
66. Obst, S. and H. Bradaczek, *Molecular Dynamics Study of the Structure and Dynamics of the Hydration Shell of Alkaline and Alkaline-Earth Metal Cations*. The Journal of Physical Chemistry, 1996. **100**(39): p. 15677-15687.

**Supporting Information “A Molecular Dynamics Study on CO₂
Diffusion Coefficient in Saline Water in a Wide Range of
Temperatures, Pressures, and Salinity Concentrations: Implications
to CO₂ Geological Storage”**

Sina Omrani^{a,‡}, Mehdi Ghasemi^{b,‡}, Saeed Mahmoodpour^{c,*}, Ali Shafiei^{a,*}, Behzad
Rostami^b

^a *Institute of Petroleum Engineering, College of Engineering, University of Tehran, Tehran, Iran.*

^b *Petroleum Engineering Program, School of Mining & Geosciences, Nazarbayev University, Nur-Sultan, Astana
010000, Kazakhstan*

^c *Institute of Applied Geosciences, Geothermal Science and Technology, Technische Universität Darmstadt,
Darmstadt, Germany*

[‡] *S. Omrani and M.Ghasemi contributed equally to this work.*

^{*} *Corresponding author*

E-mail address: ali.shafiei@nu.kz.edu (A. Shafiei), saeed.mahmoodpour@tu-darmstadt.de (S. Mahmoodpour)

1. Literature Review

In this section, we present a thorough review of previous studies on the CO₂ diffusion coefficient in water/brine. As time passed by, the advancement of technologies helped researchers to widen the range of their measurements. Earlier works were limited to a narrow range of temperature and pressure. Furthermore, most of them were performed in pure water conditions. In this respect, various methods were applied, such as the Pressure Decay method [1-3], Taylor Dispersion method [4], Raman Spectroscopy [5, 6], Microfluidic method [7], Nuclear Magnetic Resonance (NMR) [8], Molecular dynamics (MD) simulation [9, 10], etc. **Table S4** lists these studies. We pointed out some of them with more novelty in the original manuscript.

Table S4- Previous research outcomes on CO₂ diffusion coefficient measurement in water/brine. Note that T and P are temperature and pressure, respectively.

Year	Researcher	Solution (g/L)	T (K)	P (MPa)	Diffusion Coefficient ($\times 10^{-9} \frac{m^2}{s}$)
1956	Scriven et al. [11]	pure water	298	-	1.87
1961	Woods et al. [12]	pure water	298	-	1.95
1964	Tang and Himmelblau [13]	pure water	298	0.1	1.92
1964	Vivian and King [14]	pure water	298	-	2
1964	Unver and Himmelblau [15]	pure water	298	0.1	1.85
1965	Thomas and Adams [16]	pure water	298	0.1	1.95
1967	Ferrell and Himmelblau [17]	pure water	298	-	1.92
1988	Renner [3]	brine	311	1.544-5.832	1.92
1994	Tamimi et al. [18]	pure water	293-368	1	1.76-8.20
1996	Frank et al. [19]	pure water	298-328	1	1.97-3.67
1996	Wang et al. [20]	brine	311	1.524-5.178	2.925-4.827
1997	Hirai et al. [21]	pure water	286	29.4, 39.2	1.35, 1.45
2005	Tewes and Boury [22]	pure water	313	3.0-9.0	0.47-1.8
2006	Yang et al. [23]	brine	300, 330	1.786-5.647	170.7-269.8

2009	Farajzadeh et al. [24]	brine	303	1.0-5.0	2-280
2012	Nazari Moghaddam et al. [25]	pure water	298	2.185-5.861	9.07-9.86
2012	Sell et al. [7]	pure water, brine	299	0.5-5.0	1.86, 0.55-1.4
2012	Garcia-Rates et al. [9]	brine	333-453	5.0-50.0	2.4-12.55
2013	Azin et al. [2]	brine	305-325	5.9-6.9	3.52-6.16
2013	Lu et al. [5]	pure water	268-473	10.0-45.0	0.76-16.1
2013	Wang et al. [26]	brine	423	3.43-8.02	238.35-251.34
2014	Cadogan et al. [4]	pure water	298-423	14.2-49.3	2.218-12.33
2014	Moultos et al. [10]	pure water	298-623	0.1-100.0	2-55
2015	Zhang et al. [27]	brine	298-343	0.5-1.17	1.2-1.91
2015	Cadogan et al. [8]	pure water, brine	298	0.1	1.25-2.13
2015	Belgodere et al. [6]	brine	294	4.0	0.92-1.71
2015	Raad et al. [2]	pure water, brine	303, 313	5.880-6.265	0.678-23.3
2017	Zarghami et al. [28]	brine	323-348	1.745	3.6-8.2
2018	Shi et al. [29]	brine	323	6.0	1.25-82
2021	Li et al. [30]	brine	313-373	8.28-30.94	0.0166-0.0961

2. Accuracy Evaluation of Combined Force Fields

At the first stage, due to the existence of various models for CO₂ and NaCl, MD simulations have been carried out to determine the most accurate combined model. After some preliminary assessment, TraPPE [31], TraPPE (Flex) [32], EPM2 [33] models were considered for CO₂, while models developed by Smith et al. [34] and Joung and Cheatham [35] were regarded for NaCl. Moreover, according to the literature, the SPC/E model was assumed for water molecules [36]. In summary, 6 different combined models, namely TraPPE-SPC/E-Smith, EPM2-SPC/E-Smith, TraPPE-SPC/E-JC, EPM2-SPC/E-JC, TraPPE (Flex)-SPC/E-Smith, and TraPPE (Flex)-SPC/E-JC, were selected to compare the result of the self-diffusion coefficient obtained by MD simulations

with available experimental data measured by Belgodere et al. [6] in distinct NaCl molarities of 1, 2, and 3. To evaluate and compare the accuracy of combined models with the measured values in a laboratory, various statistical analyses, including average percent relative error (APRE), average percent absolute relative error (AAPRE), standard deviation (SD) of error, and root mean square error (RSME) and coefficient of determination (R^2) [37]. The average value of the self-diffusion coefficient (3 times repetition) for different molarities is shown in **Table S5**. It should be noted that the employed simulation procedure was explained in the original manuscript. Also, the results of statistical analyses are revealed in

Table S6. As is clear, the most accurate model is TraPPE (Flex)-SPC/E-JC, which was adopted for the rest of the simulations.

Table S5- The average value of the self-diffusion coefficient for 6 different combined models. Note that (A) TraPPE-SPC/E-Smith, (B) EPM2-SPC/E-Smith, (C) TraPPE-SPC/E-JC, (D) EPM2-SPC/E-JC, (E)TraPPE (Flex)-SPC/E-Smith, and (F) TraPPE (Flex)-SPC/E-JC

	1 M	2 M	3 M
Ref. [6]	1.5500	1.3800	1.2900
A	1.8440	1.6326	1.2940
B	1.6966	1.6033	1.3757
C	1.7415	1.6080	1.2080
D	1.7720	1.5553	1.1500
E	1.7122	1.5812	1.2780
F	1.6831	1.5164	1.3210

Table S6- Statistical error analysis of 6 different combined models. Note that (A) TraPPE-SPC/E-Smith, (B) EPM2-SPC/E-Smith, (C) TraPPE-SPC/E-JC, (D) EPM2-SPC/E-JC, (E) TraPPE (Flex)-SPC/E-Smith, and (F) TraPPE (Flex)-SPC/E-JC.

Analyses	Molarity	A	B	C	D	E	F
APRE	1	-18.9677	-9.4623	-12.3548	-14.3225	-9.6312	-9.3322
	2	-18.3091	-9.4623	-16.5217	-13.7053	-14.5246	-9.2864

	3	-0.3100	-6.6149	6.3565	7.8527	-0.8123	-1.0542
	T	-12.5289	-8.5132	-7.5066	-6.7250	-8.3227	-6.5576
AAPRE	1	0.2940	0.1466	0.1915	0.2220	0.1748	0.1546
	2	0.2526	0.2233	0.2280	0.1753	0.2230	0.1842
	3	0.0580	0.0853	0.1080	0.1400	0.0430	0.0640
	T	0.2015	0.1517	0.1758	0.7911	0.1470	0.1343
RMSE	1	0.3170	0.1760	0.2002	0.2421	0.1866	0.1925
	2	0.2665	0.2350	0.2400	0.2102	0.2125	0.2232
	3	0.0687	0.0901	0.1356	0.1568	0.0801	0.0542
	T	0.2174	0.1670	0.1919	0.2030	0.1597	0.1598
SD	1	0.2505	0.1391	0.1826	0.1913	0.1745	0.2151
	2	0.2365	0.2485	0.2459	0.1865	0.1945	0.2066
	3	0.0652	0.0855	0.1486	0.1489	0.0756	0.0342
	T	0.1841	0.1577	0.1924	0.1756	0.1482	0.1520
R ²	1	0.9135	0.9784	0.9633	0.9457	0.9735	0.9749
	2	0.9361	0.9501	0.9480	0.9893	0.9794	0.9814
	3	0.9999	0.9927	0.9932	0.9867	0.9897	0.9981
	T	0.9499	0.9737	0.9682	0.9739	0.9809	0.9848

3. Assessment of the Effect of Box Size on the Diffusion Coefficient

Various researchers have investigated the finite-size effect of the diffusion coefficient computed by molecular dynamics simulations [38, 39]. A common method of checking the effect of box size is to run simulations in boxes of different lengths and measure the difference between them [10]. The objective is to measure the diffusion coefficient at the thermodynamic limit, or, in other words, to compute diffusion coefficients in an infinite box ($1/L \rightarrow 0$). Three simulation box sizes were considered: 3, 4.5, and 7 nm.

Figure S14 shows the results. As it can be seen, compared to each other, there is not much of a difference.

This fact is confirmed by calculating the Yeh–Hummer correction term [40]. It also shows that the required correction is minor (almost two orders of magnitude lower than the diffusion coefficient).

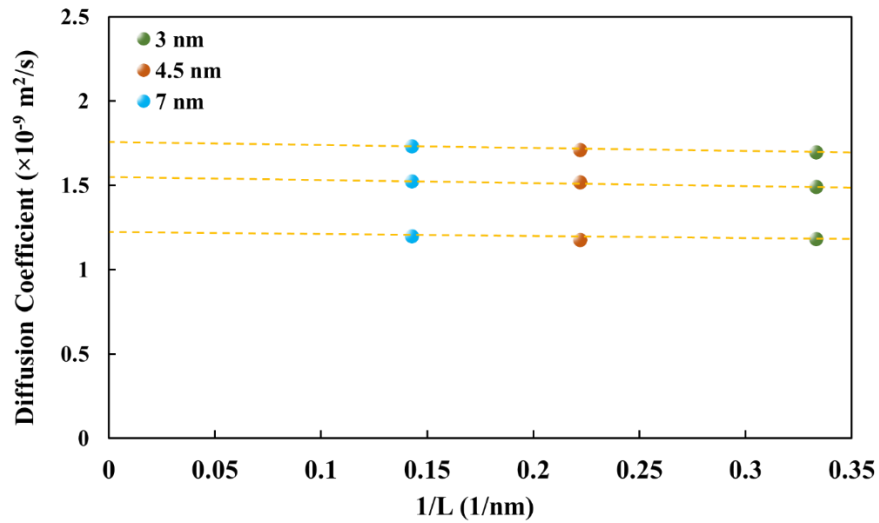
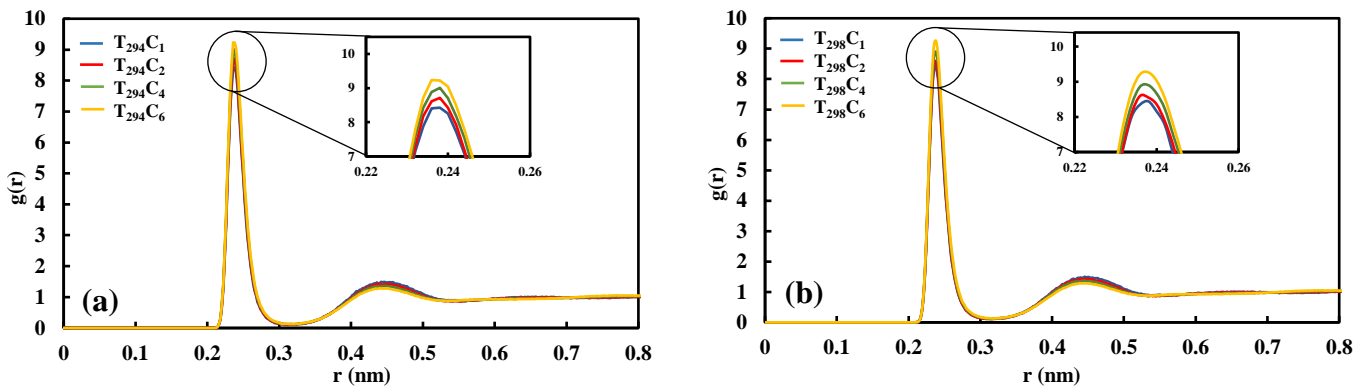


Figure S14. The CO₂ diffusion coefficient at 294 K and 10 MPa in the box with the length of 3 (green), 4.5 (Orange), and 7 (blue) nm.

4. Results of RDFs

The RDFs of all investigated pairs are shown hereunder. However, only two cases of 294 K and 423 K are shown in the original manuscript.



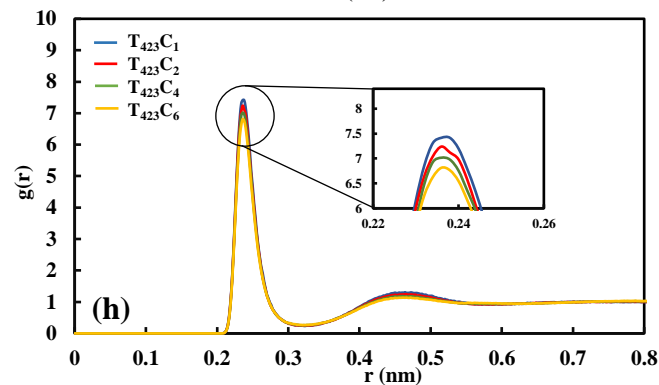
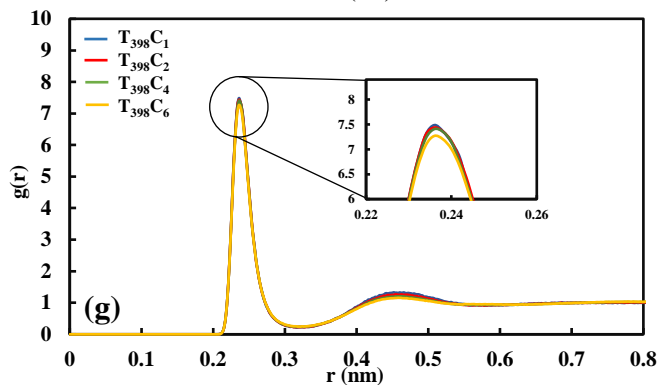
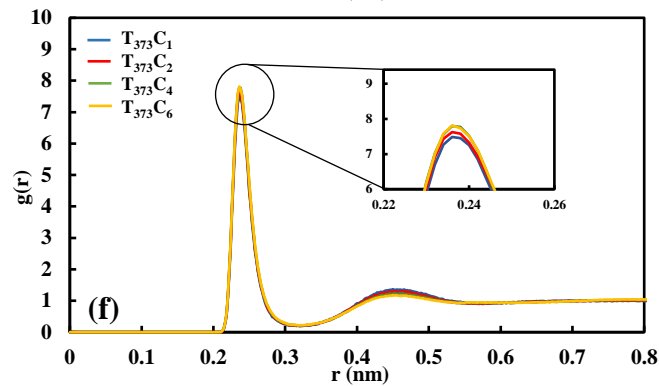
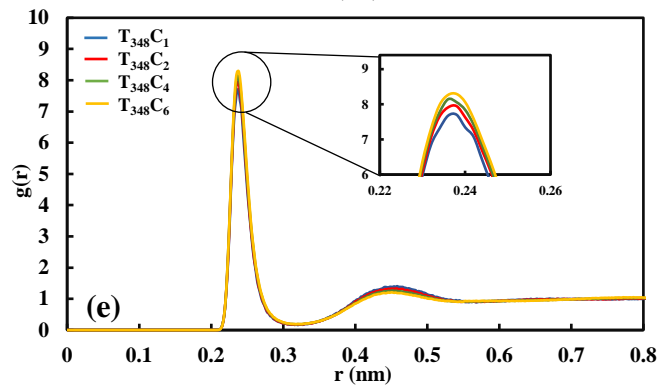
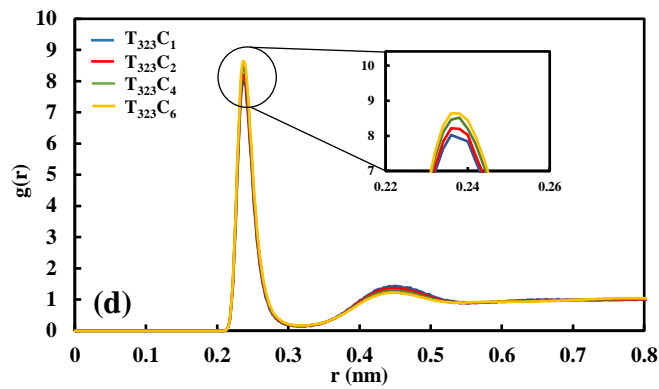
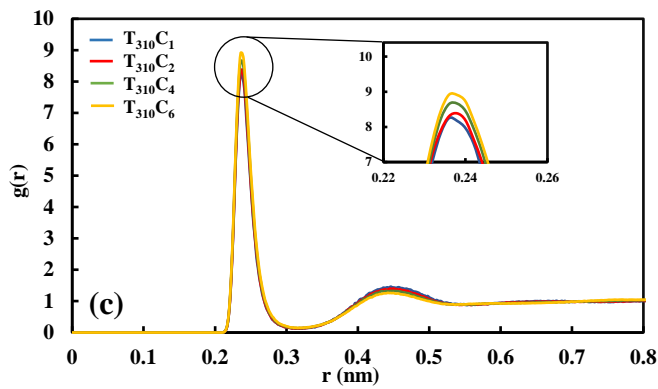
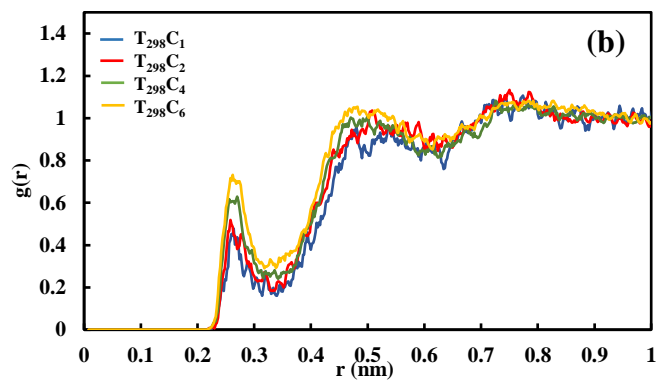
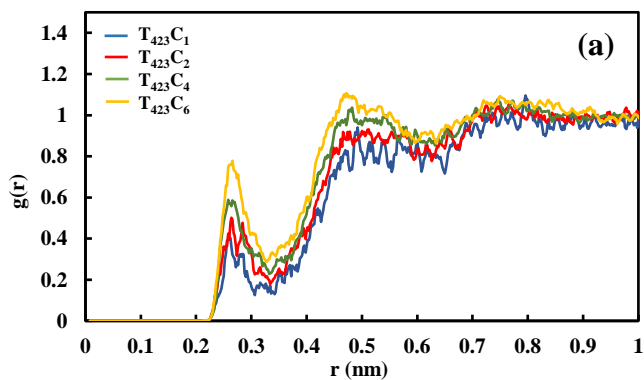


Figure S15- RDF curves of $Na-O_{H_2O}$ in various NaCl solutions at the temperatures of (a) 294 K, (b) 298 K, (c) 310 K, (d) 323 K, (e) 348 K, (f) 373, (g) 398 K, and (h) 423 K.



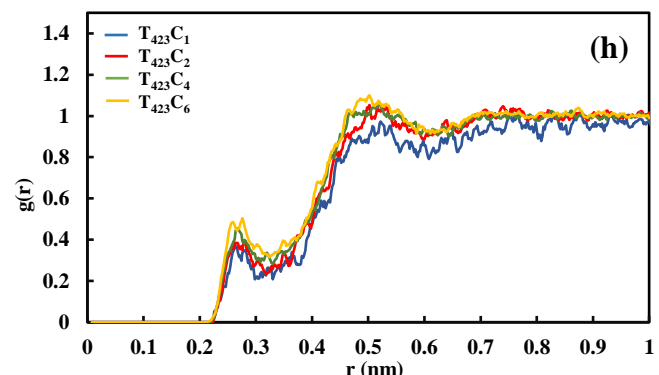
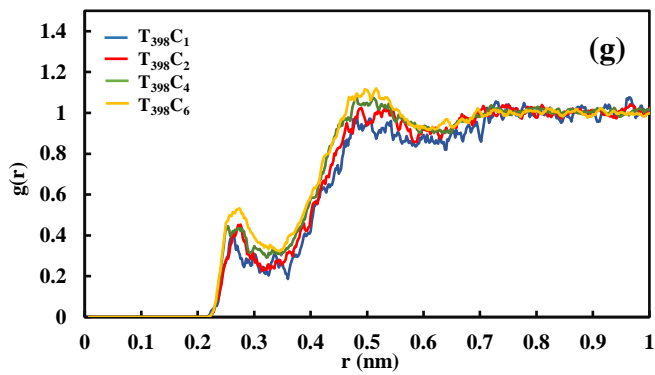
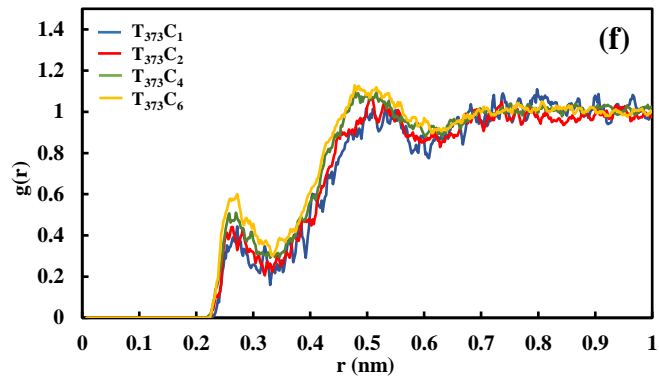
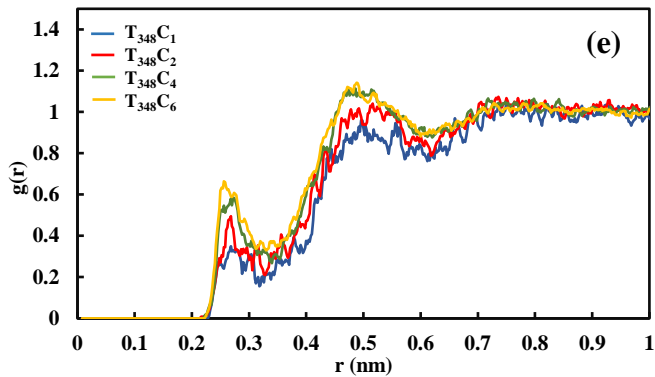
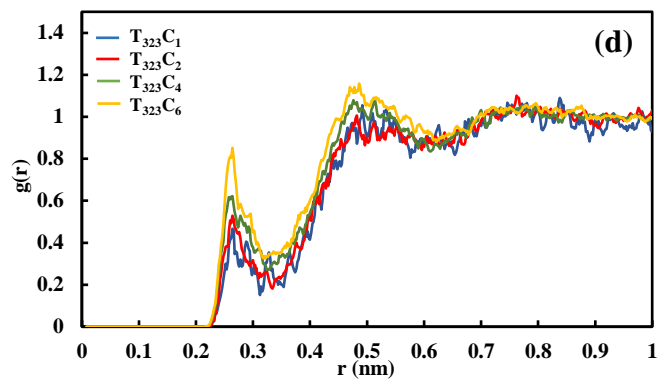
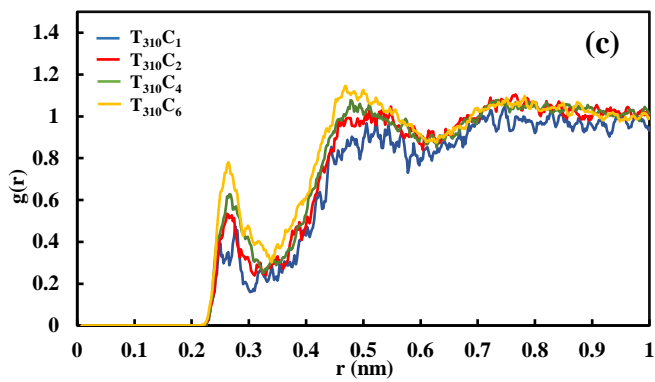
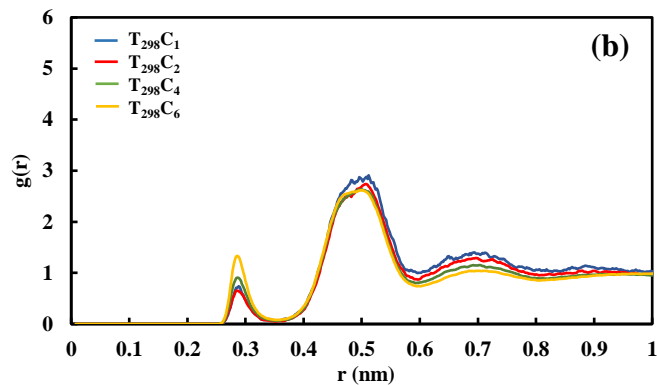
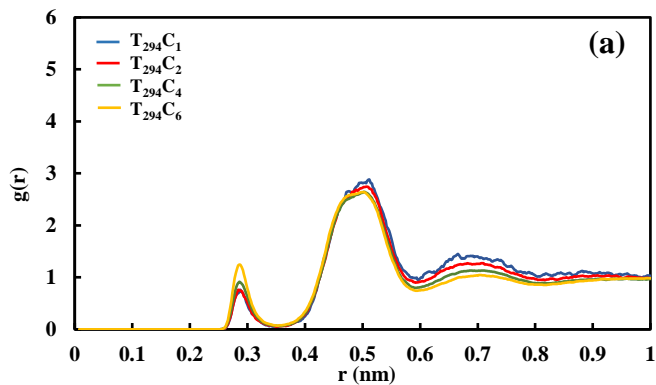


Figure S16- RDF curves of $Na-O_{CO_2}$ in various NaCl solutions at the temperatures of (a) 294 K, (b) 298 K, (c) 310 K, (d) 323 K, (e) 348 K, (f) 373 K, (g) 398 K, and (h) 423 K.



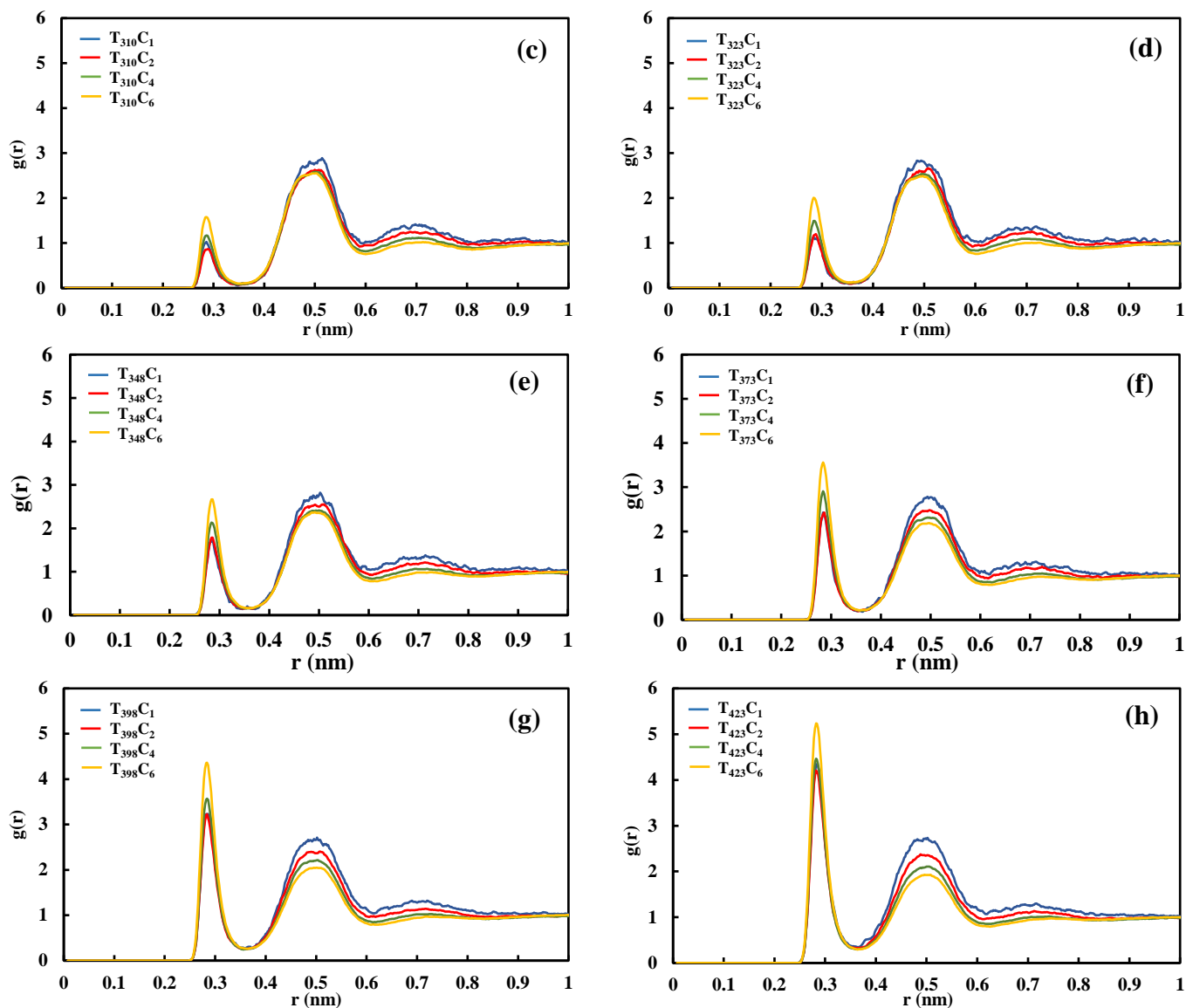
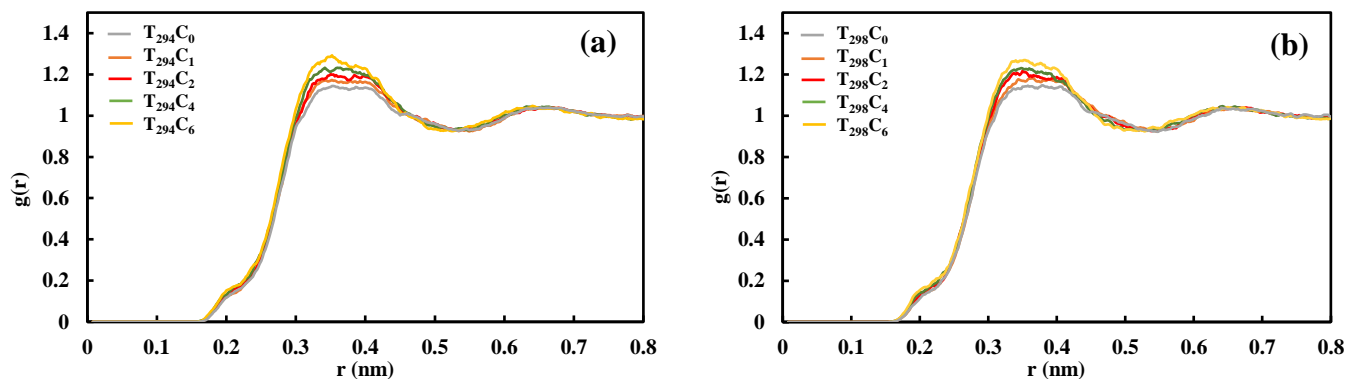


Figure S17- RDF curves of *Na-Cl* in various NaCl solutions at the temperatures of (a) 294 K, (b) 298 K, (c) 310 K, (d) 323 K, (e) 348 K, (f) 373 K, (g) 398 K, and (h) 423 K.



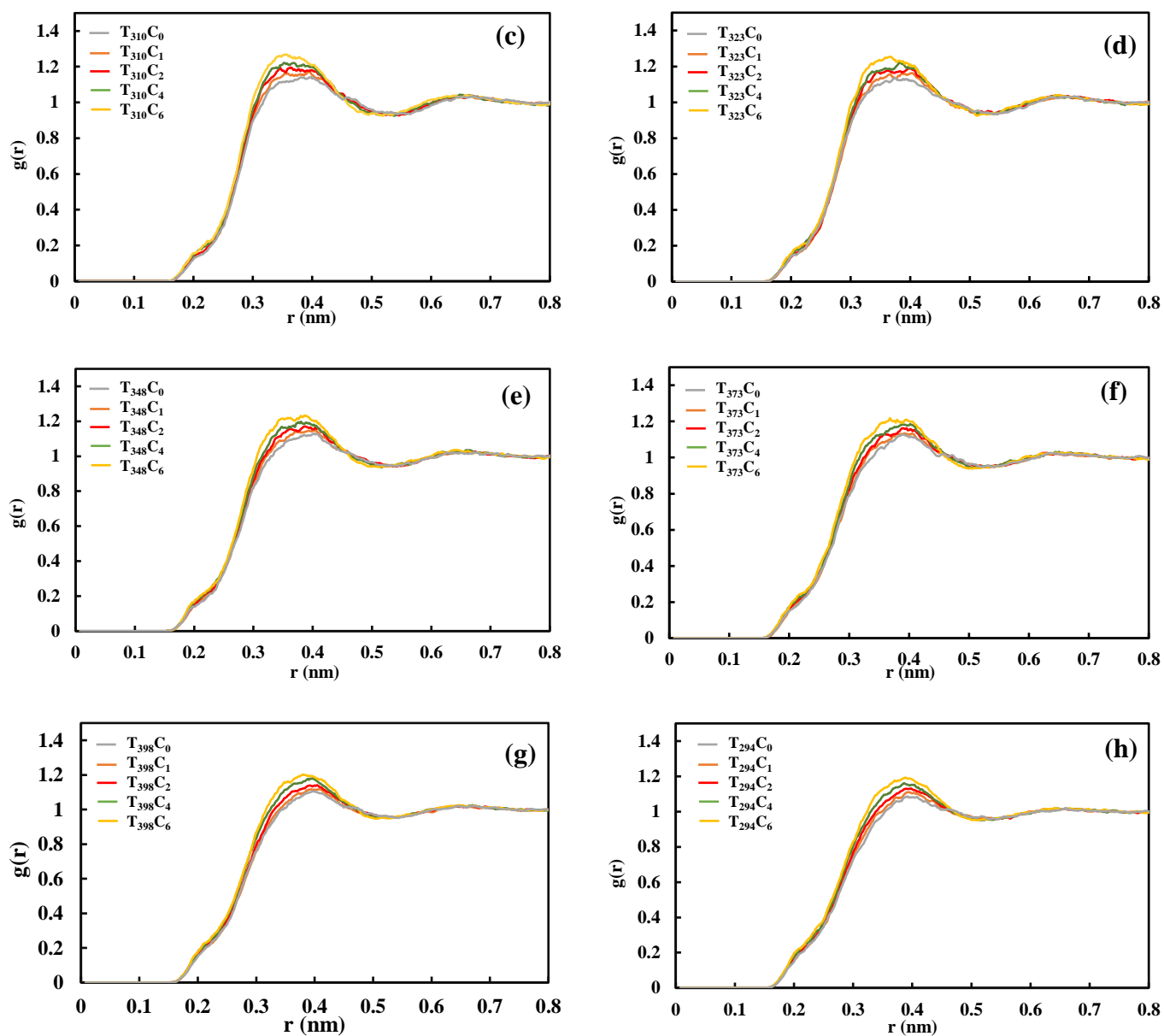


Figure S18-RDF curves of O_{CO_2} - H_2O in various aqueous solutions at the temperatures of (a) 294 K, (b) 298 K, (c) 310 K, (d) 323 K, (e) 348 K, (f) 373 K, (g) 398 K, and (h) 423 K.

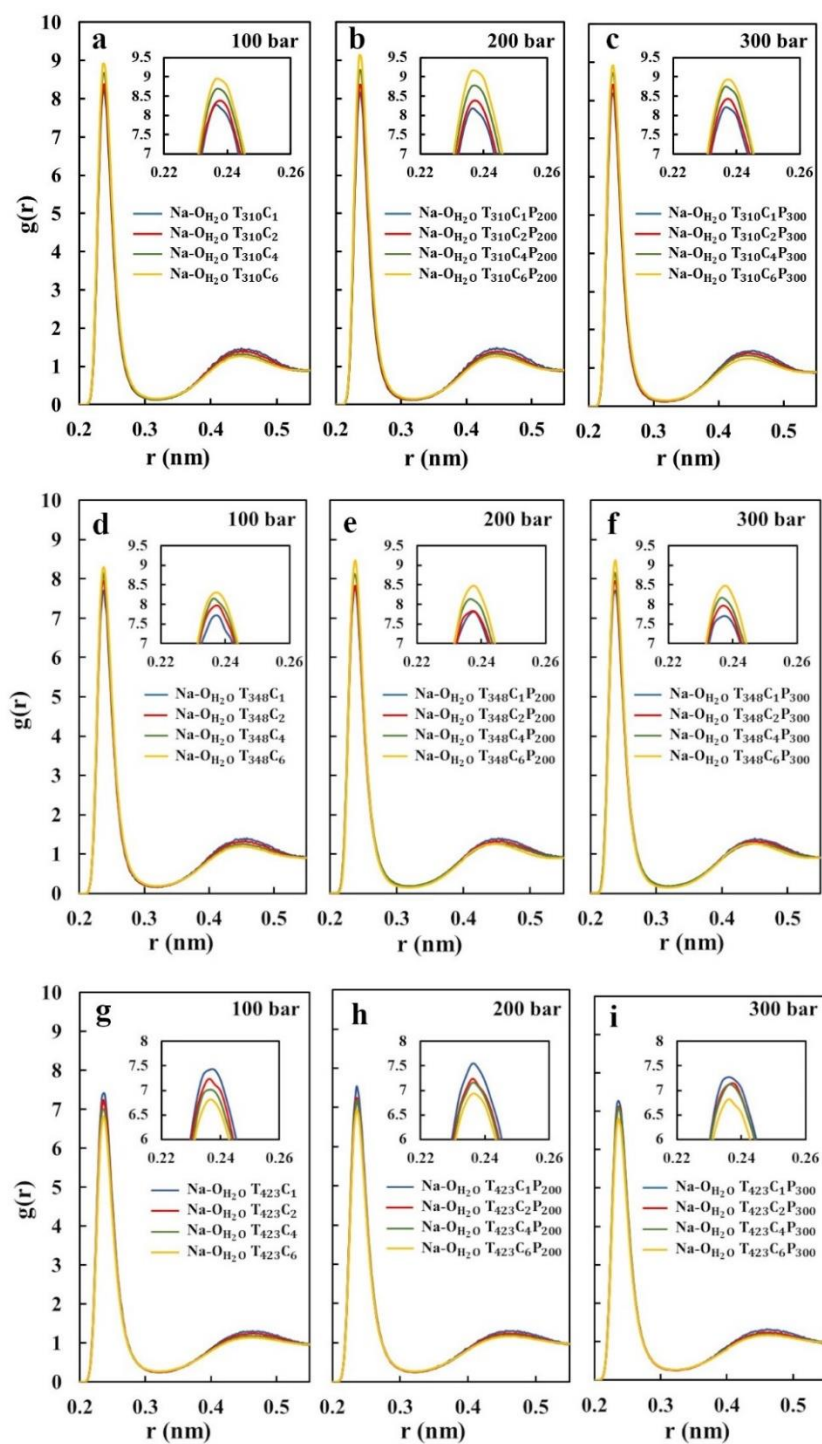


Figure S19- RDF values between Na- O_{H_2O} at 310 K and pressures of a) 100 bar b) 200 bar c) 300 bar, at 348 K and pressures of d) 100 bar, e) 200 bar, and f) 300 bar, and at 423 K and pressures of g) 100 bar, h) 200 bar, and i) 300 bar.

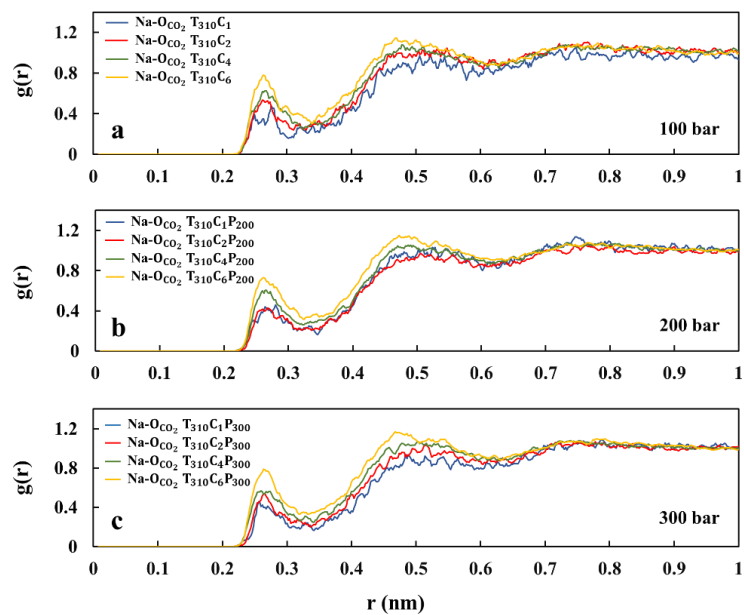


Figure S20- RDF values between Na- O_{CO_2} at 310 K and pressures of a) 100 bar b) 200 bar c) 300 bar.

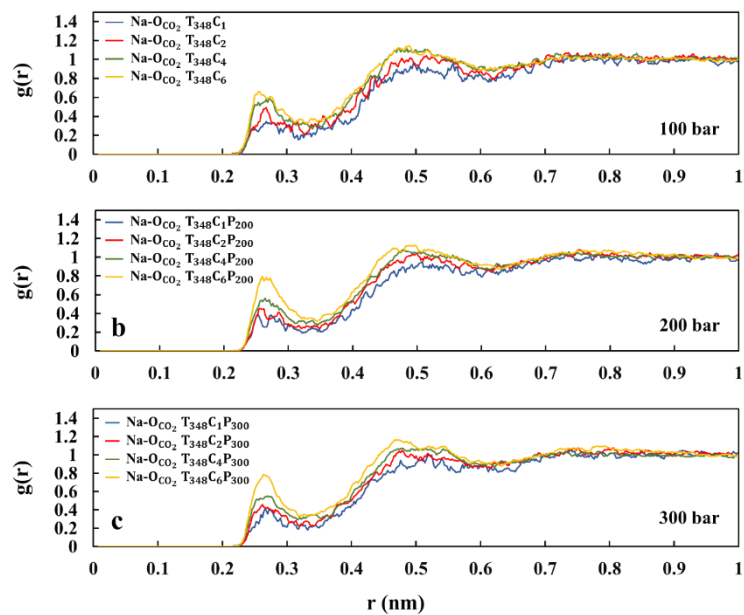


Figure S21- RDF values between Na- O_{CO_2} at 348 K and pressures of a) 100 bar, b) 200 bar, and c) 300 bar.

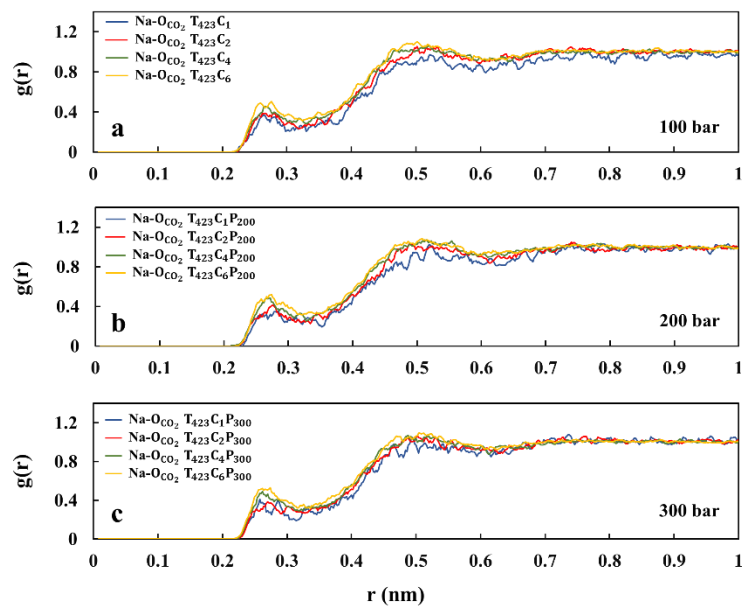


Figure S22- RDF values between $\text{Na-O}_{\text{CO}_2}$ at 423 K and pressure of a) 100 bar, b) 200 bar, and c) 300 bar.

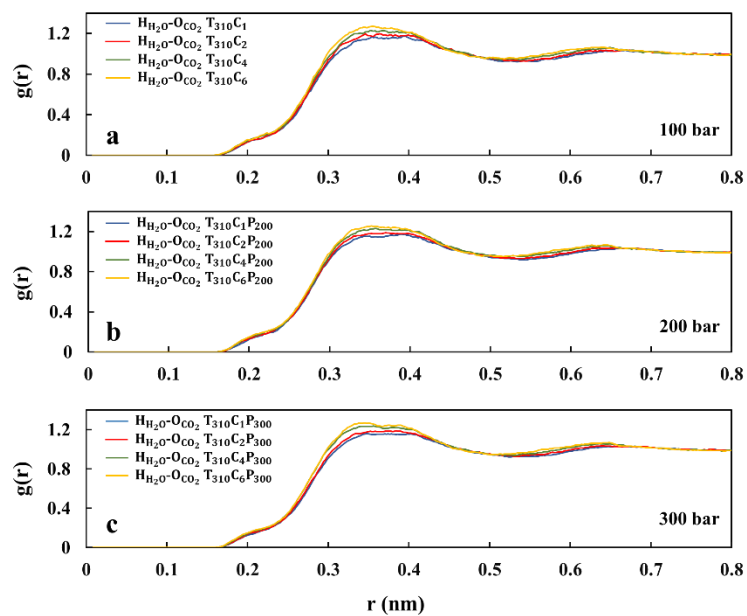


Figure S23- RDF values between $\text{H}_{2\text{O}}-\text{O}_{\text{CO}_2}$ at 310 K and pressure of a) 100 bar, b) 200 bar, and c) 300 bar

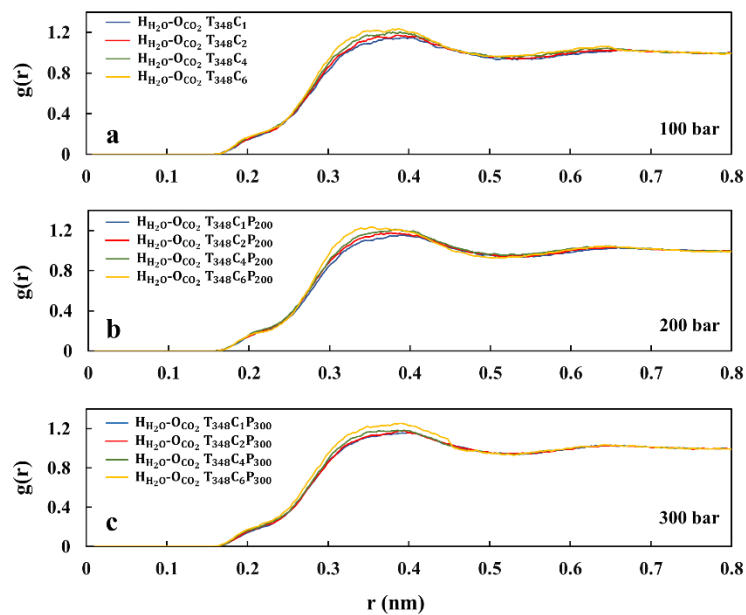


Figure S24- RDF values between $H_{2}O-O_{CO_2}$ at 348 K and pressure of a) 100 bar, b) 200 bar, and c) 300 bar

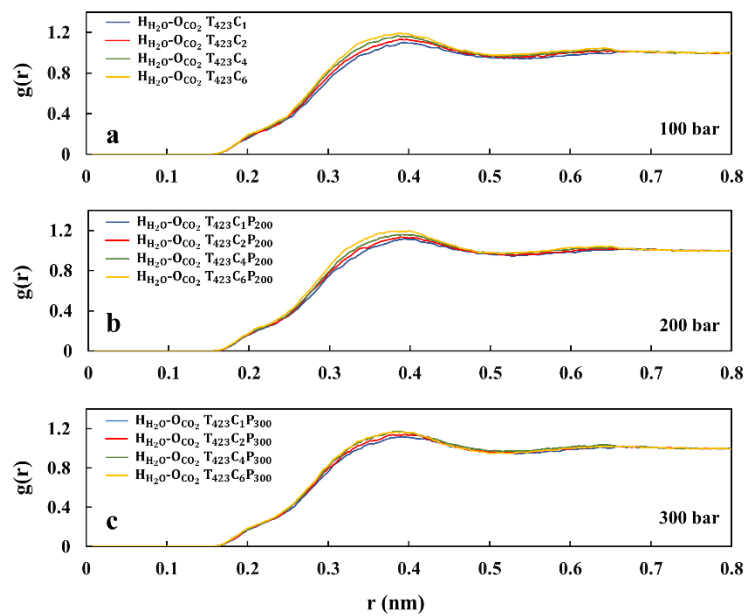


Figure 25- RDF values between $H_{2}O-O_{CO_2}$ at 423 K and pressure of a) 100 bar, b) 200 bar, and c) 300 bar

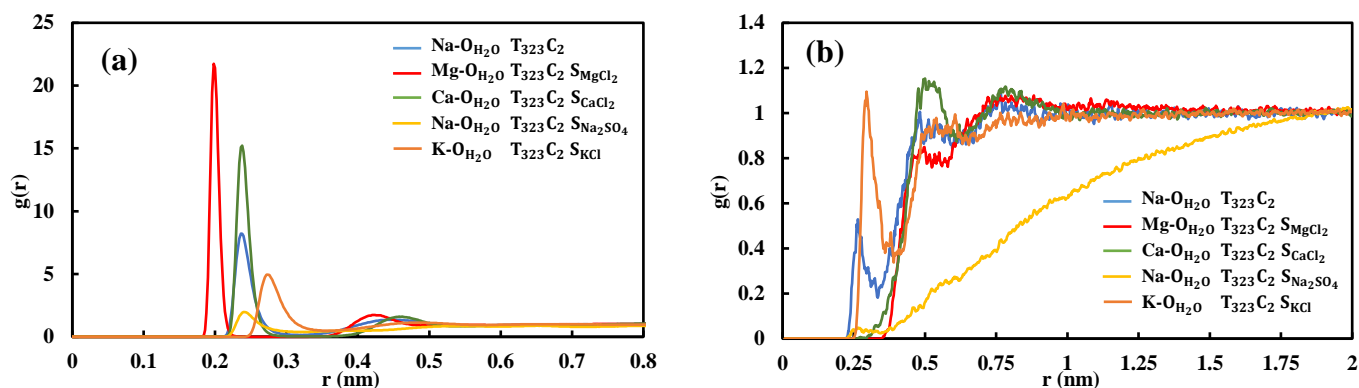


Figure S26- The RDF values between cations and (a) O_{H_2O} and (b) O_{CO_2} in various saline solutions at the temperatures 323 K and 2 M concentration.

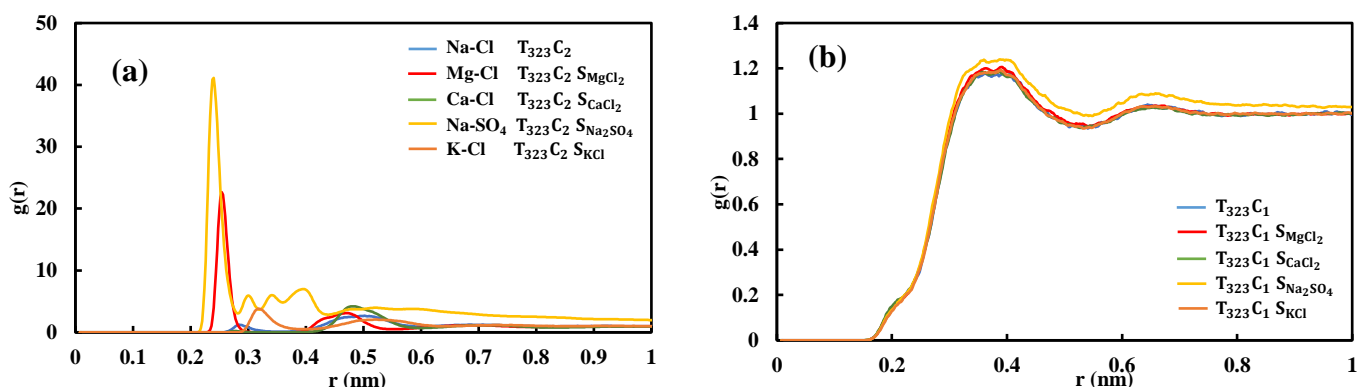


Figure S27- The RDF values between (a) cations-anions and (b) $H_{H_2O}-O_{H_2O}$ in various saline solutions at the temperatures 323 K and 2 M concentration.

References

- [1] Azin R, Mahmoudy M, Raad SMJ, Osfouri S. Measurement and modeling of CO₂ diffusion coefficient in saline aquifer at reservoir conditions. Central European Journal of Engineering. 2013;3:585-94. <https://doi.org/10.2478/s13531-012-0069-2>.
- [2] Raad SMJ, Azin R, Osfouri S. Measurement of CO₂ diffusivity in synthetic and saline aquifer solutions at reservoir conditions: the role of ion interactions. Heat and Mass Transfer. 2015;51:1587-95. <https://doi.org/10.1007/s00231-015-1508-4>.
- [3] Renner T. Measurement and correlation of diffusion coefficients for CO₂ and rich-gas applications. SPE reservoir engineering. 1988;3:517-23. <https://doi.org/10.2118/15391-PA>.

- [4] Cadogan SP, Maitland GC, Trusler JM. Diffusion coefficients of CO₂ and N₂ in water at temperatures between 298.15 K and 423.15 K at pressures up to 45 MPa. *Journal of Chemical & Engineering Data*. 2014;59:519-25. <https://doi.org/10.1021/je401008s>.
- [5] Lu W, Guo H, Chou I-M, Burruss R, Li L. Determination of diffusion coefficients of carbon dioxide in water between 268 and 473 K in a high-pressure capillary optical cell with in situ Raman spectroscopic measurements. *Geochimica et Cosmochimica Acta*. 2013;115:183-204. <https://doi.org/10.1016/j.gca.2013.04.010>.
- [6] Belgodere C, Dubessy J, Vautrin D, Caumon MC, Sterpenich J, Pironon J, et al. Experimental determination of CO₂ diffusion coefficient in aqueous solutions under pressure at room temperature via Raman spectroscopy: impact of salinity (NaCl). *Journal of Raman Spectroscopy*. 2015;46:1025-32. <https://doi.org/10.1002/jrs.4742>.
- [7] Sell A, Fadaei H, Kim M, Sinton D. Measurement of CO₂ diffusivity for carbon sequestration: A microfluidic approach for reservoir-specific analysis. *Environmental science & technology*. 2013;47:71-8. <https://doi.org/10.1021/es303319q>.
- [8] Cadogan SP, Hallett JP, Maitland GC, Trusler JM. Diffusion coefficients of carbon dioxide in brines measured using ¹³C pulsed-field gradient nuclear magnetic resonance. *Journal of Chemical & Engineering Data*. 2015;60:181-4. <https://doi.org/10.1021/je5009203>.
- [9] Garcia-Rates M, de Hemptinne J-C, Avalos JB, Nieto-Draghi C. Molecular modeling of diffusion coefficient and ionic conductivity of CO₂ in aqueous ionic solutions. *The Journal of Physical Chemistry B*. 2012;116:2787-800. <https://doi.org/10.1021/jp2081758>.
- [10] Moulton OA, Tsimpanogiannis IN, Panagiotopoulos AZ, Economou IG. Atomistic molecular dynamics simulations of CO₂ diffusivity in H₂O for a wide range of temperatures and pressures. *The Journal of Physical Chemistry B*. 2014;118:5532-41. <https://doi.org/10.1021/jp502380r>.
- [11] SCRIVEN II LE. *Interfacial resistance in gas absorption*: University of Delaware; 1956.
- [12] Woods DR. *Mass Transfer Between a Liquid Jet and a Counter-current Gas Stream*: University of Wisconsin--Madison; 1961.

- [13] Tang Y, Himmelblau D. Effect of solute concentration on the diffusivity of carbon dioxide in water. *Chemical Engineering Science*. 1965;20:7-14. [https://doi.org/10.1016/0009-2509\(65\)80038-0](https://doi.org/10.1016/0009-2509(65)80038-0).
- [14] Vivian JE, King CJ. Diffusivities of slightly soluble gases in water. *AIChE Journal*. 1964;10:220-1. <https://doi.org/10.1002/aic.690100217>.
- [15] Unver A, Himmelblau D. Diffusion Coefficients of CO₂, C₂H₄, C₃H₆ and C₄H₈ in Water from 6 to 65 C. *Journal of Chemical & Engineering Data*. 1964;9:428-31. <https://doi.org/10.1021/je60022a043>.
- [16] Thomas W, Adams M. Measurement of the diffusion coefficients of carbon dioxide and nitrous oxide in water and aqueous solutions of glycerol. *Transactions of the Faraday Society*. 1965;61:668-73. <https://doi.org/10.1039/TF9656100668>.
- [17] Ferrell RT, Himmelblau DM. Diffusion coefficients of nitrogen and oxygen in water. *Journal of chemical and engineering data*. 1967;12:111-5. <https://doi.org/10.1021/je60032a036>.
- [18] Tamimi A, Rinker EB, Sandall OC. Diffusion coefficients for hydrogen sulfide, carbon dioxide, and nitrous oxide in water over the temperature range 293-368 K. *Journal of Chemical and Engineering data*. 1994;39:330-2. <https://doi.org/10.1021/je00014a031>.
- [19] Frank MJ, Kuipers JA, van Swaaij WP. Diffusion coefficients and viscosities of CO₂+ H₂O, CO₂+ CH₃OH, NH₃+ H₂O, and NH₃+ CH₃OH liquid mixtures. *Journal of chemical & engineering data*. 1996;41:297-302. <https://doi.org/10.1021/je950157k>.
- [20] Wang L-S, Lang Z-X, Guo T-M. Measurement and correlation of the diffusion coefficients of carbon dioxide in liquid hydrocarbons under elevated pressures. *Fluid Phase Equilibria*. 1996;117:364-72. [https://doi.org/10.1016/0378-3812\(95\)02973-7](https://doi.org/10.1016/0378-3812(95)02973-7).
- [21] Hirai S, Okazaki K, Yazawa H, Ito H, Tabe Y, Hijikata K. Measurement of CO₂ diffusion coefficient and application of LIF in pressurized water. *Energy*. 1997;22:363-7. [https://doi.org/10.1016/S0360-5442\(96\)00135-1](https://doi.org/10.1016/S0360-5442(96)00135-1).
- [22] Tewes F, Bours F. Formation and Rheological Properties of the Supercritical CO₂- Water Pure Interface. *The Journal of Physical Chemistry B*. 2005;109:3990-7. <https://doi.org/10.1021/jp046019w>.

- [23] Yang C, Gu Y. Accelerated mass transfer of CO₂ in reservoir brine due to density-driven natural convection at high pressures and elevated temperatures. *Industrial & engineering chemistry research*. 2006;45:2430-6. <https://doi.org/10.1021/ie050497r>.
- [24] Farajzadeh R, Ranganathan P, Zitha P, Bruining J. The effect of heterogeneity on the character of density-driven natural convection of CO₂ overlying a brine layer. *Canadian Unconventional Resources and International Petroleum Conference: OnePetro*; 2010. <https://doi.org/10.2118/138168-MS>.
- [25] Moghaddam RN, Rostami B, Pourafshary P, Fallahzadeh Y. Quantification of density-driven natural convection for dissolution mechanism in CO₂ sequestration. *Transport in porous media*. 2012;92:439-56. <https://doi.org/10.1007/s11242-011-9911-x>.
- [26] Wang S, Hou J, Liu B, Zhao F, Yuan G, Liu G. The pressure-decay method for nature convection accelerated diffusion of CO₂ in oil and water under elevated pressures. *Energy Sources, Part A: Recovery, Utilization, and Environmental Effects*. 2013;35:538-45. <https://doi.org/10.1080/15567036.2012.705415>.
- [27] Zhang J, Clennell MB, Liu K, Dewhurst DN, Pervukhina M, Sherwood N. Molecular dynamics study of CO₂ sorption and transport properties in coal. *Fuel*. 2016;177:53-62. <https://doi.org/10.1016/j.fuel.2016.02.075>.
- [28] Zarghami S, Boukadi F, Al-Wahaibi Y. Diffusion of carbon dioxide in formation water as a result of CO₂ enhanced oil recovery and CO₂ sequestration. *Journal of Petroleum Exploration and Production Technology*. 2017;7:161-8. <https://doi.org/10.1007/s13202-016-0261-7>.
- [29] Shi Z, Wen B, Hesse M, Tsotsis T, Jessen K. Measurement and modeling of CO₂ mass transfer in brine at reservoir conditions. *Advances in water resources*. 2018;113:100-11. <https://doi.org/10.1016/j.advwatres.2017.11.002>.
- [30] Li Z, Yuan L, Sun G, Lv J, Zhang Y. Experimental Determination of CO₂ Diffusion Coefficient in a Brine-Saturated Core Simulating Reservoir Condition. *Energies*. 2021;14:540. <https://doi.org/10.3390/en14030540>.
- [31] Potoff JJ, Siepmann JJ. Vapor-liquid equilibria of mixtures containing alkanes, carbon dioxide, and nitrogen. *AIChE journal*. 2001;47:1676-82. <https://doi.org/10.1002/aic.690470719>.

- [32] Perez-Blanco ME, Maginn EJ. Molecular dynamics simulations of CO₂ at an ionic liquid interface: Adsorption, ordering, and interfacial crossing. *The Journal of Physical Chemistry B*. 2010;114:11827-37. <https://doi.org/10.1021/jp103862v>.
- [33] Harris JG, Yung KH. Carbon dioxide's liquid-vapor coexistence curve and critical properties as predicted by a simple molecular model. *The Journal of Physical Chemistry*. 1995;99:12021-4. <https://doi.org/10.1021/j100031a034>.
- [34] Smith DE, Dang LX. Computer simulations of NaCl association in polarizable water. *The Journal of Chemical Physics*. 1994;100:3757-66. <https://doi.org/10.1063/1.466363>.
- [35] Joung IS, Cheatham III TE. Determination of alkali and halide monovalent ion parameters for use in explicitly solvated biomolecular simulations. *The journal of physical chemistry B*. 2008;112:9020-41. <https://doi.org/10.1021/jp8001614>.
- [36] Berendsen H, Grigera J, Straatsma T. The missing term in effective pair potentials. *Journal of Physical Chemistry*. 1987;91:6269-71. <https://doi.org/10.1021/j100308a038>.
- [37] Ershadnia R, Amooie MA, Shams R, Hajirezaie S, Liu Y, Jamshidi S, et al. Non-Newtonian fluid flow dynamics in rotating annular media: Physics-based and data-driven modeling. *Journal of Petroleum Science and Engineering*. 2020;185:106641. <https://doi.org/10.1016/j.petrol.2019.106641>.
- [38] Celebi AT, Jamali SH, Bardow A, Vlught TJ, Moulτος OA. Finite-size effects of diffusion coefficients computed from molecular dynamics: a review of what we have learned so far. *Molecular Simulation*. 2020:1-15. <https://doi.org/10.1080/08927022.2020.1810685>.
- [39] Jamali SH, Bardow A, Vlught TJ, Moulτος OA. Generalized form for finite-size corrections in mutual diffusion coefficients of multicomponent mixtures obtained from equilibrium molecular dynamics simulation. *Journal of chemical theory and computation*. 2020;16:3799-806. <https://doi.org/10.1021/acs.jctc.0c00268>.
- [40] Dünweg B, Kremer K. Molecular dynamics simulation of a polymer chain in solution. *The Journal of chemical physics*. 1993;99:6983-97. <https://doi.org/10.1063/1.465445>.